X. DEEP-SEA SEDIMENTS IN THE GH79-1 AREA: THEIR GEOLOGICAL PROPERTIES

Akira Nishimura

Introduction

In this chapter, a sediment lithology including surface features observed by bottom photography is described, and its geological meaning is discussed. Sampling apparatus used and numbers of sampling are as follows.

1) Double spades box corer (G(B)) at 39 stations.
2) Large box corer with single spade (G(B′)) at 3 stations.
3) Freefall grab with small sampling tube (FG) at 166 times, always associated with dredge, box corer, piston corer, and deep-sea camera.
4) Piston corer (P) at 5 stations.
5) Dredge (D) at one station.
6) Bottom photography by means of one-shot camera attached to freefall grab (FG-C) at 115 times, one-shot camera attached to large box corer (G(B′)-C) at one station, and continuous-shot deep-sea camera (C) at one station.

Bottom sediments sampled by box corer and piston corer were handled through the procedure shown in Fig. X-1. Lithologic type was determined by two methods, smear slide observation and composition analysis using sedimentation tube (ARITA, 1977). The former method was used for all samples including sediments from the sampling tube attached to freefall grab, whereas the latter for the samples from the box corer and piston corer. Content of the sand-sized grain was generally determined by volumetric ratio of the coarse fraction ($>63\mu$) by sedimentation tube method, because the volumetric ratio coincides with the weight ratio of sediment except for siliceous ooze (NAKAO, 1979). Lithologic type was classified according to the content of biogenic component and authigenic mineral component (Table X-1), which was estimated by volumetric ratios of sand-sized fraction and smear slide observation. The components of sediment were distinguished as follows.

biogenic component
- 1-i.* radiolaria
- ii.* diatom
- iii.* silicoflagellata†
- iv.* spine (sponge spicule and radiolarian spine)
- v.**foraminifera
- vi.**calcareous nannoplankton†
- vii. ichthyolith

authigenic mineral component
- 2-i. zeolite
- ii. manganese micronodule

*1-i to 1-iv; siliceous microfossils.
**1-v to 1-vi; calcareous microfossils.
†detected only under smear slide observation.

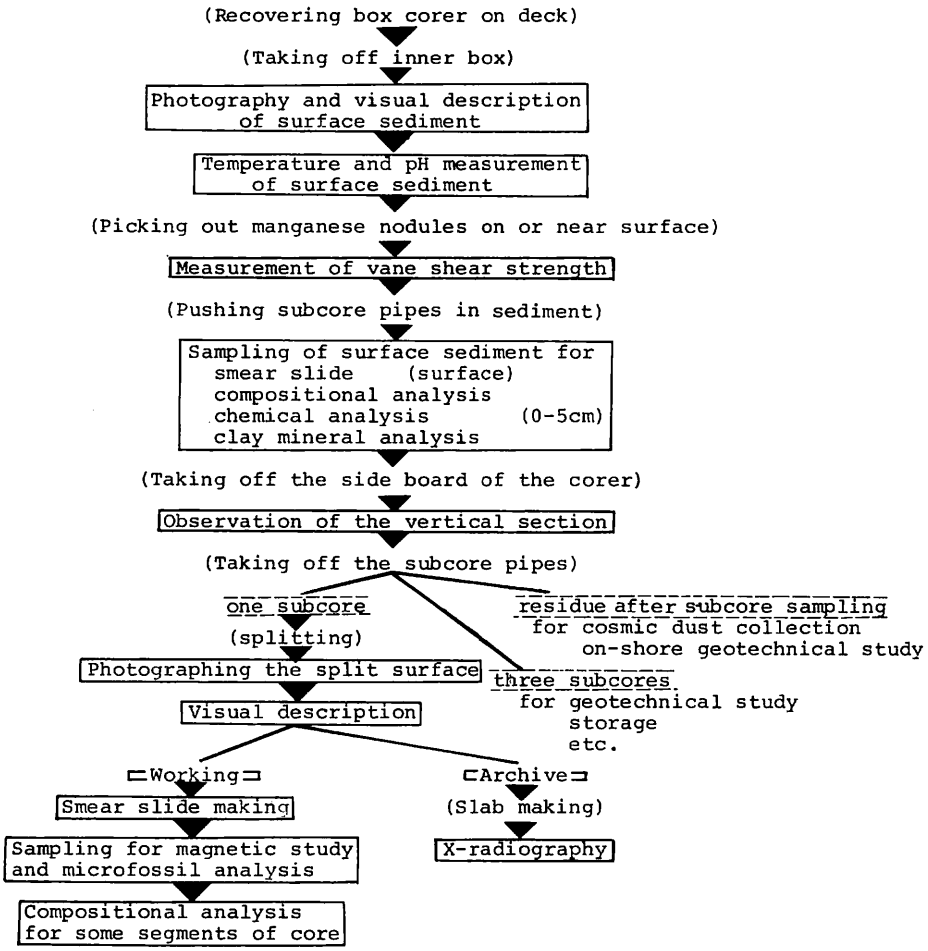

Fig. X-1 (1)

Fig. X-1 Procedure of handling box core and piston core materials.

Table X-1 Framework of sediment classification.

Clay		
Zeolite rich clay 5%<*zeolite*<10%	Siliceous fossil rich clay 5%<*siliceous fossil*<10%	Calcareous fossil rich clay 5%<*calcareous fossil*<10%
Zeolitic clay 10%<*zeolite*	Siliceous clay 10%<*siliceous fossil*<30%	Calcareous clay 10%<*calcareous fossil*<30%
	Siliceous ooze 30%<*siliceous fossil*	Calcareous ooze 30%<*calcareous fossil*

siliceous fossil; radiolarians, diatom, silicoflagellates, and spines.
calcareous fossil; foraminifers and calcareous nannoplankton.

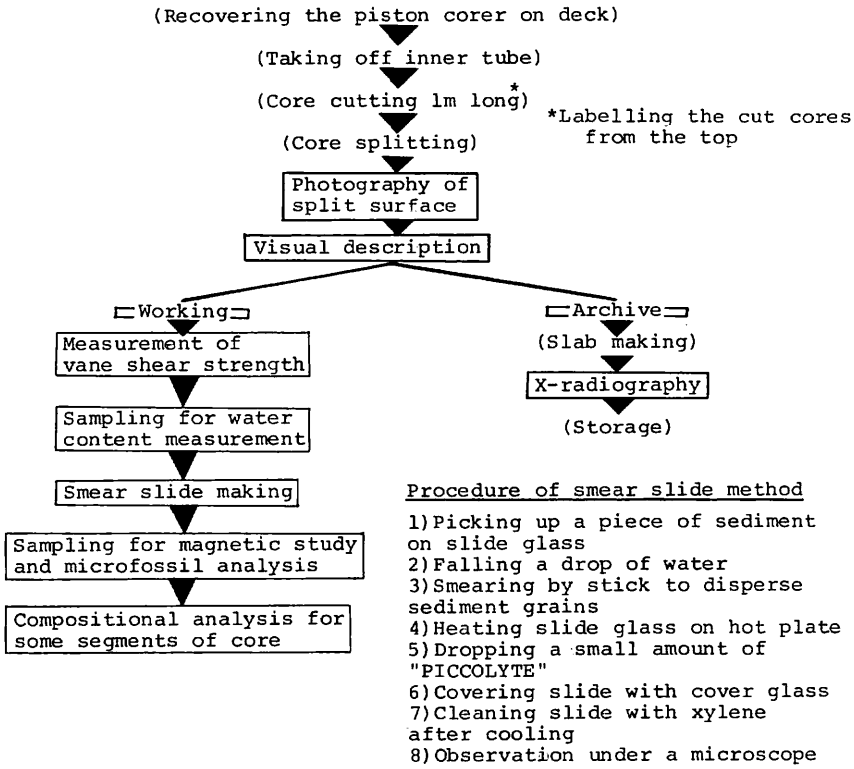

Fig. X-1 (2)

Age of sediments was estimated by two methods, microfossil analysis and paleomagnetic study. Microfossil analysis of radiolarians, ichthyoliths, calcareous nannoplankton, and planktonic foraminifers, were done on some selected samples. Some representative forms identified are illustrated in Fig. X-11(1–4). Paleomagnetic measurements were made on all piston core samples (JOSHIMA, this cruise report).

Descriptions of sediment and results of analysis are made on separated two parts, the GH79–1 main survey area and the detailed survey area. These areas are shown in Fig. X-2. Near these area, there are Sites 170 and 165 of DSDP which offer useful data to construct the geological history of the entire survey area and its environs.

Sediments in the GH79–1 main survey area

Surficial sediment* distribution is shown in Fig. X-3. Based on lithology of surficial sediment this area is divided into four provinces, topographically higher, western, central, and eastern provinces.

The topographically higher province is shallower than 5,000 m, on and around seamounts in the western and central southern parts of this area, and is dominated by

*In this chapter, surficial sediment is defined as uppermost part (0–5 cm) of bottom sediment. Its distribution was outlined mainly by box core samples. The sediments in the sampling tube attached to freefall grab assisted to deduce the distribution at the area without box core sediment. Sediment in the tube seems to have been taken from about 10 cm below sea bottom.

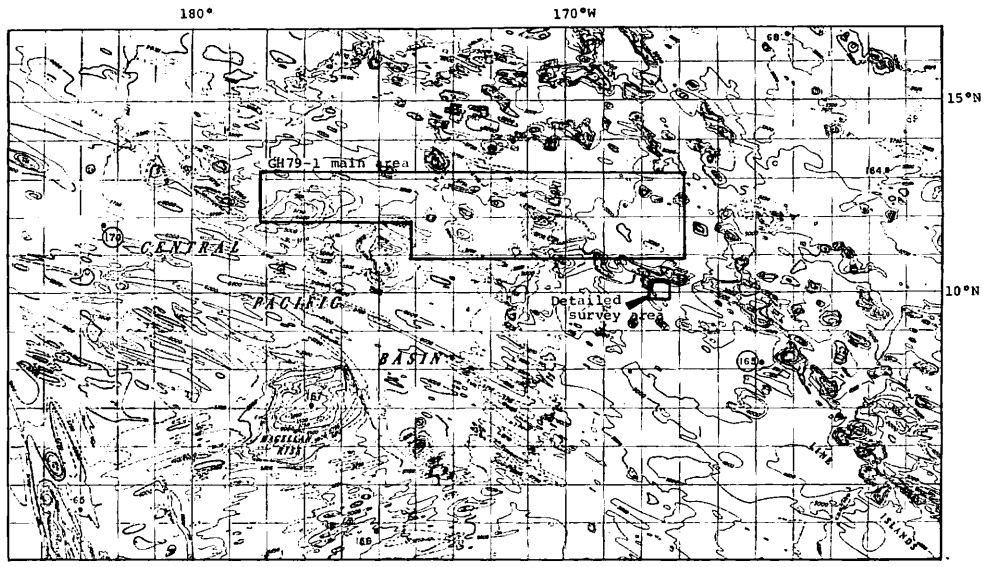

Fig. X-2 Survey areas of GH79-1 and DSDP sites. Topographic map after WINTERER, EWING, *et al.* (1973).

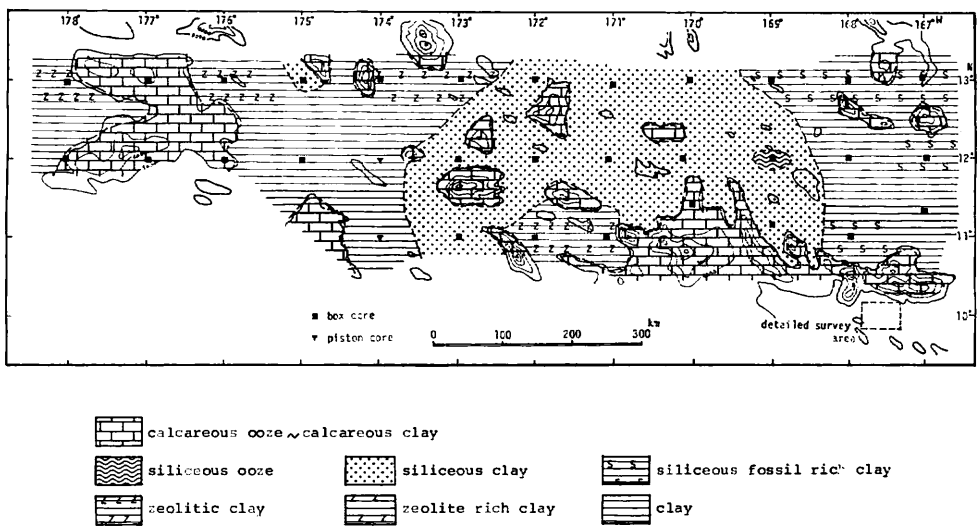

Fig. X-3 Surficial sediment distribution of the GH79-1 main survey area.

calcareous sediments, very pale brown calcareous ooze and calcareous clay. The main composition of coarse fraction is planktonic foraminiferal tests. Microscopic observation of smear slides also shows high content of calcareous nannoplankton. The contrast of lithology between this province and other provinces without calcareous organism tests, is formed by the difference of dissolution degree of calcareous organism tests related to calcium carbonate compensation depth.

Surficial sediment of the western province (178°–173°W) is dominantly dark brown clay and zeolitic clay. The main composition of coarse fraction is zeolite and radiolarians. The sediments commonly contain cross-shaped phillipsite crystals and spherical zeolite aggregations.

Surficial sediment of the central province (173°–169°W) is dominantly brown siliceous clay. This province continues southwardly to the adjacent area (ARITA, 1977). The main composition of coarse fraction is radiolarians.

The eastern province (169°–167°W) appears to be covered dominantly by dark brown clay and siliceous fossil rich clay. The main composition of coarse fraction is radiolarians. However, the conclusions are somewhat subtle, because sediment sampling by box corer was missed in some stations.

Small distribution of siliceous ooze is found in the eastern cental part of this area. The main composition of coarse fraction is siliceous microfossils, radiolarian tests and diatom test fragments *Ethmodiscus*.

Split subcores are illustrated in Fig. X-4.

Subcore descriptions and results of coarse fraction analysis of the sediments are shown in Fig. X-5. Vertical change of lithology is represented by changes of content and composition of coarse fraction. As for the cores with surficial sediment of calcareous ooze, no lithological change is observed throughout. As for the cores with surficial sediment of siliceous clay and siliceous fossil rich clay, the downward decreasing of coarse fraction is commonly observed. This change is caused by decreasing of siliceous organism tests, radiolarians and diatom. Consequently, the surficial siliceous clay gradually changes to clay with lower content of siliceous organism tests. Rarely, the siliceous clay is underlain by clay with sharp boundary of distinct color change (G934).

All surficial sediments are possibly the Quaternary in age because of their yielding of Quaternary radiolarians or Quaternary planktonic foraminifers. Many Tertiary radiolarians and a few Tertiary ichthyoliths are observed in subcores. In places the Tertiary (the Middle Eocene) radiolarians exceed 70 per cent of total radiolarian assemblage even in surficial sediment (Table X-2). These radiolarians are thought to be the fossils reworked into younger sediments (THEYER, 1977).

In the GH79–1 main survey area, piston cores were obtained from three stations along the 174°W meridian (Fig. X-6, X-7). These stations are in the western province of the surficial sediment dominantly of clay.

P139; (St. 1452A) Some fragmental pieces of black manganese crust were only obtained. The Oligocene to upper Cretaceous consolidated sequence reported from DSDP Site 170 (WINTERER, EWING, *et al.*, 1973), is possibly exposed and covered by manganese crust, on the basis of the absence of transparent layer on 3.5 kHz record at this station and the absence of sediment in the core.

P140; (St. 1487) Consolidated bedded dark reddish brown siltstone was obtained in the core catcher. The siltstone is accompanied by thin chalcedonic veinlets and yields a few poorly preserved radiolarians (Eocene?). It can be correlated with the Oligocene to upper Cretaceous sequence of Site 170, which is overlain by thin brown clay. In this station, dark brown to dark greyish brown clay occurs throughout the core (0–4.2 m) above the siltstone.

P141; (St. 1488) Homogeneous dark brown clay occurs throughout the core (0–4.7 m).

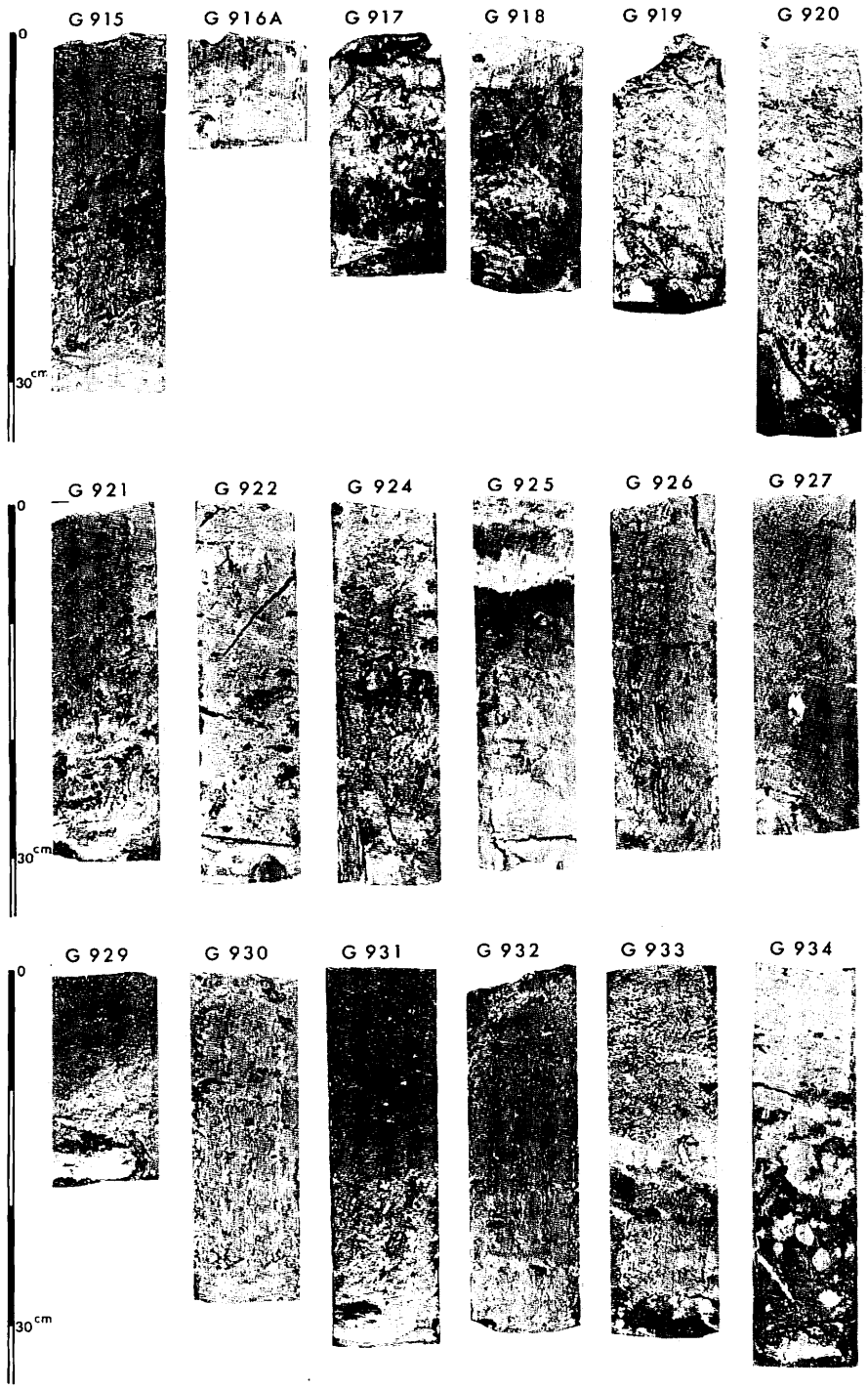

Fig. X-4 (1)

Fig. X-4 Photographs of split surface of subcores.

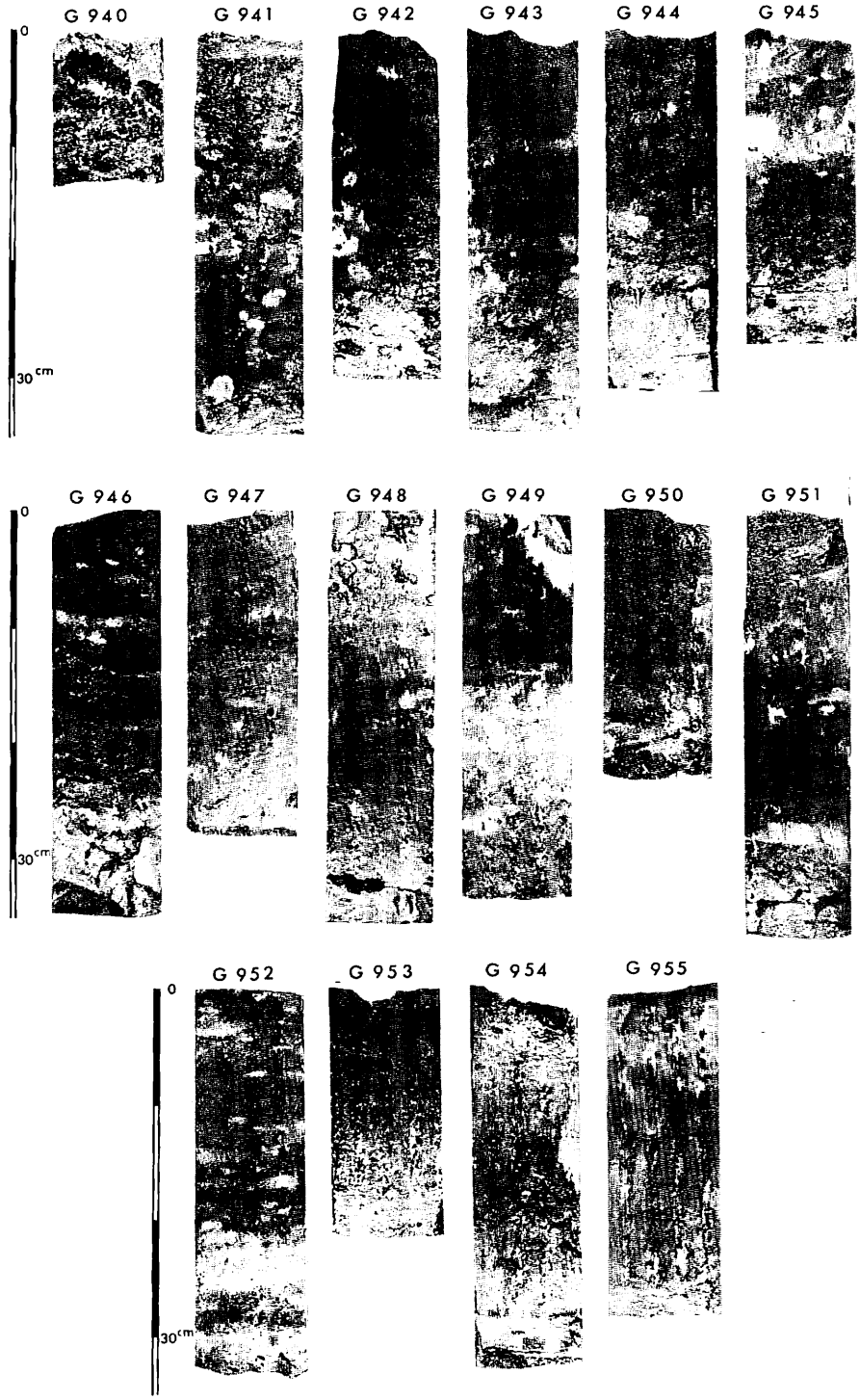
G 940
G 941
G 942
G 943
G 944
G 945
0
30 cm
G 946
G 947
G 948
G 949
G 950
G 951
0
30 cm
G 952
G 953
G 954
G 955
0
30 cm

Fig. X-4 (2)

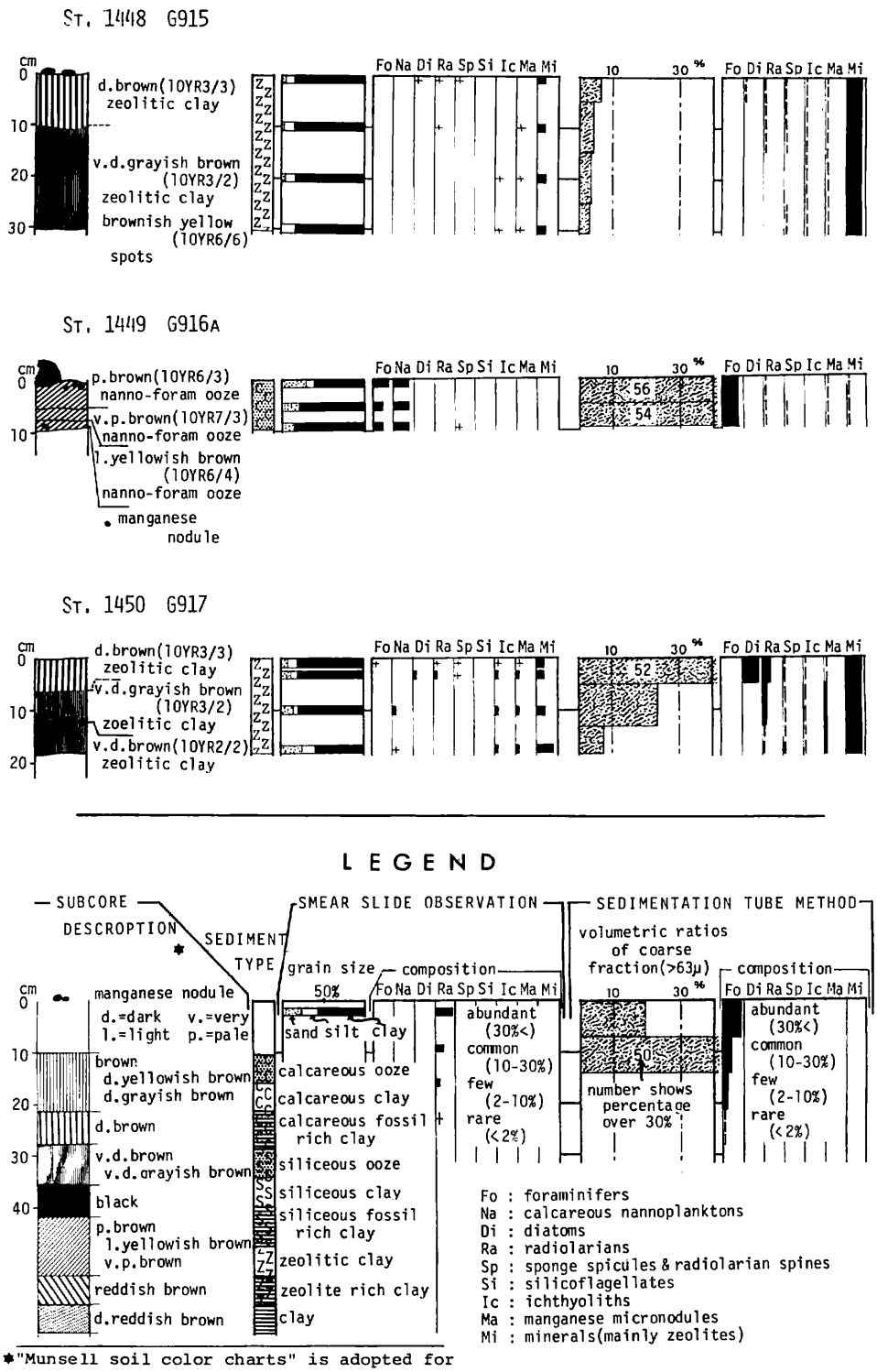

Fig. X-5 (1)

Fig. X-5 Descriptions of subcores and results of compositional analysis.

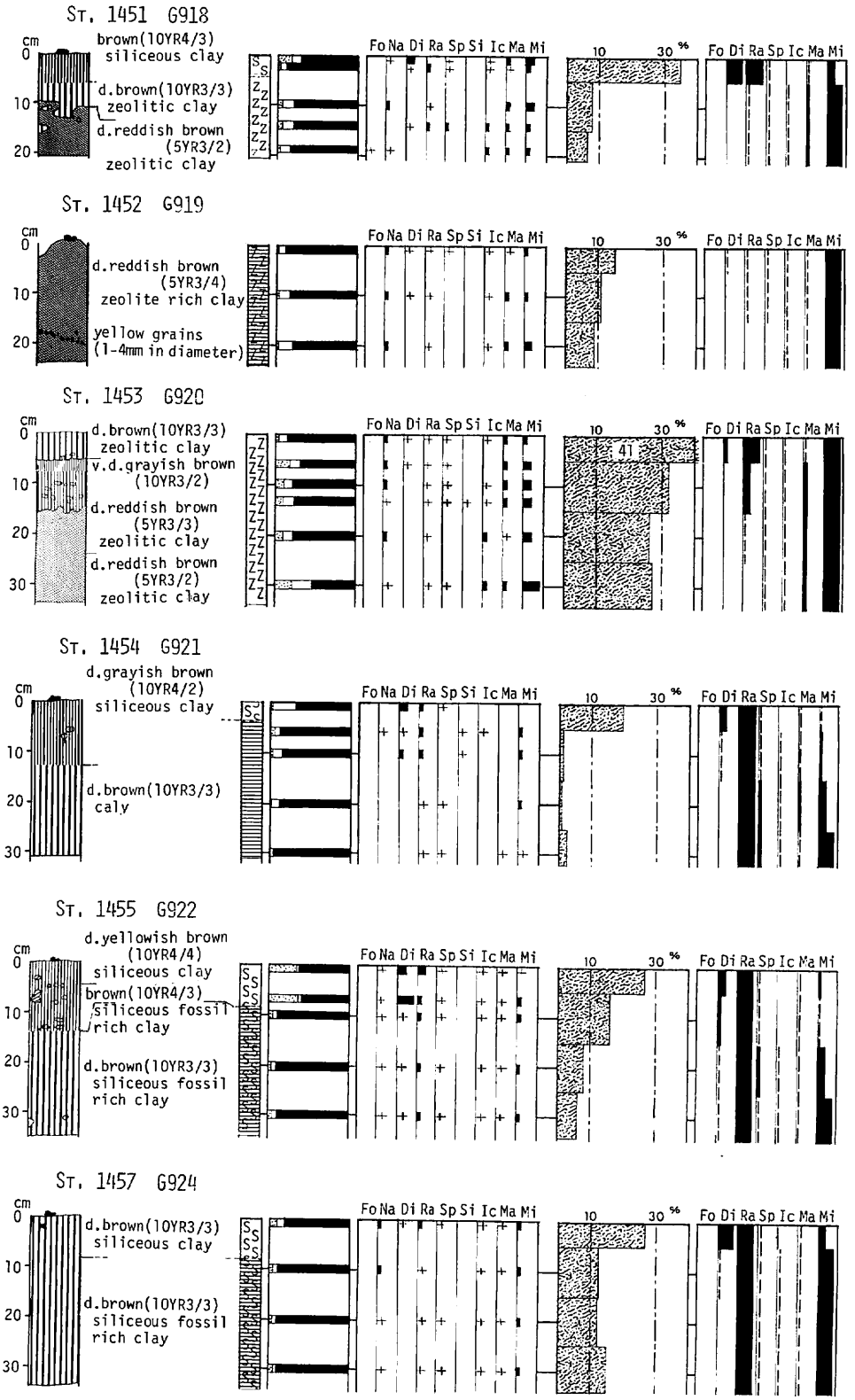
St. 1451 G918
cm
0
10
20
brown(10YR4/3) siliceous clay
d.brown(10YR3/3) zeolitic clay
d.reddish brown (5YR3/2) zeolitic clay
Fo Na Di Ra Sp Si Ic Ma Mi
10 30 %
Fo Di Ra Sp Ic Ma Mi
St. 1452 G919
cm
0
10
20
d.reddish brown (5YR3/4) zeolite rich clay
yellow grains (1-4mm in diameter)
Fo Na Di Ra Sp Si Ic Ma Mi
10 30 %
Fo Di Ra Sp Ic Ma Mi
St. 1453 G920
cm
0
10
20
30
d.brown(10YR3/3) zeolitic clay
v.d.grayish brown (10YR3/2)
d.reddish brown (5YR3/3) zeolitic clay
d.reddish brown (5YR3/2) zeolitic clay
Fo Na Di Ra Sp Si Ic Ma Mi
10 30 %
41
Fo Di Ra Sp Ic Ma Mi
St. 1454 G921
cm
0
10
20
30
d.grayish brown (10YR4/2) siliceous clay
d.brown(10YR3/3) caly
Fo Na Di Ra Sp Si Ic Ma Mi
10 30 %
Fo Di Ra Sp Ic Ma Mi
St. 1455 G922
cm
0
10
20
30
d.yellowish brown (10YR4/4) siliceous clay
brown(10YR4/3) siliceous fossil rich clay
d.brown(10YR3/3) siliceous fossil rich clay
Fo Na Di Ra Sp Si Ic Ma Mi
10 30 %
Fo Di Ra Sp Ic Ma Mi
St. 1457 G924
cm
0
10
20
30
d.brown(10YR3/3) siliceous clay
d.brown(10YR3/3) siliceous fossil rich clay
Fo Na Di Ra Sp Si Ic Ma Mi
10 30 %
Fo Di Ra Sp Ic Ma Mi

Fig. X-5 (2)

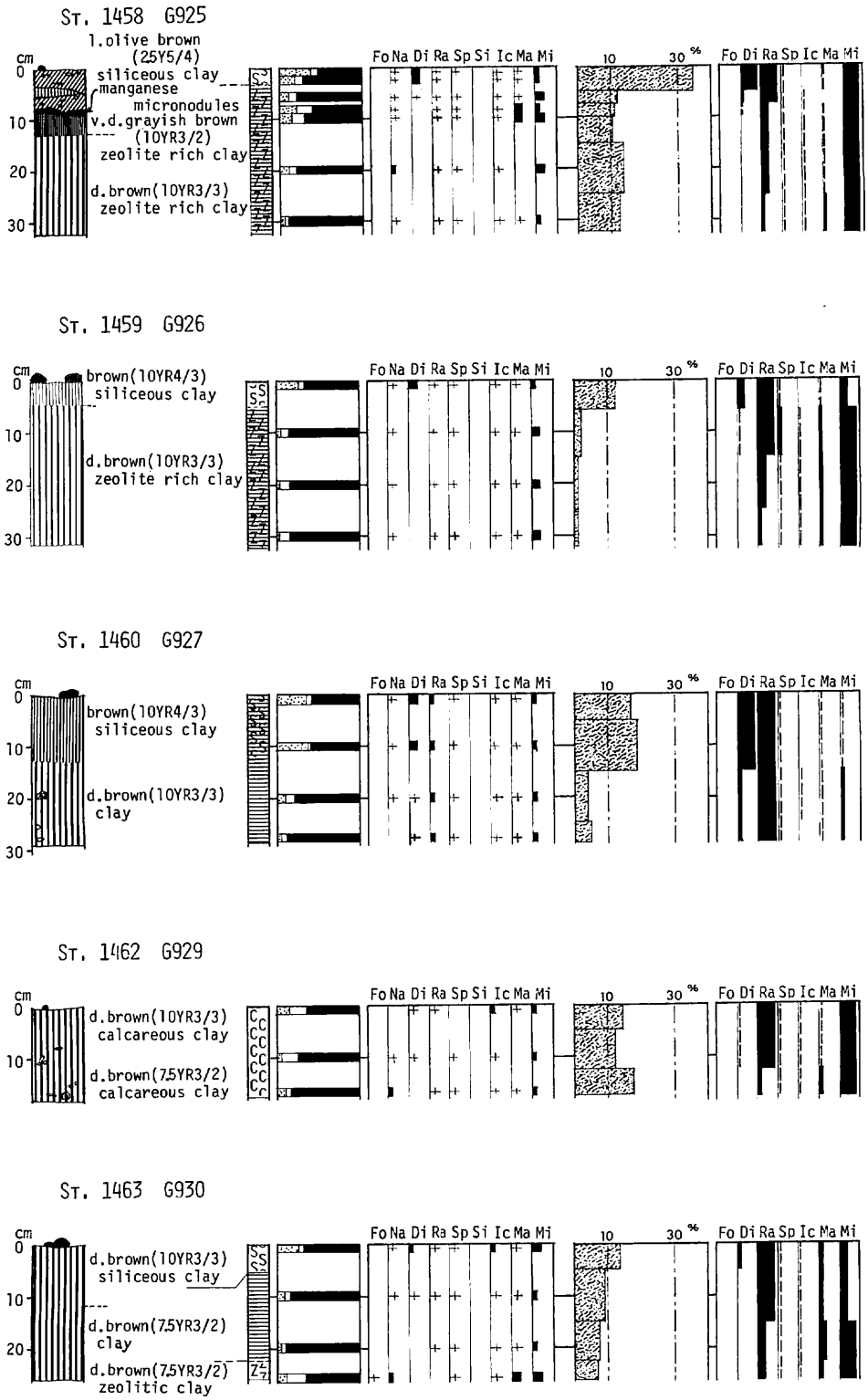
St. 1458 G925
l.olive brown (2.5Y5/4) siliceous clay
manganese micronodules
v.d.grayish brown (10YR3/2) zeolite rich clay
d.brown(10YR3/3) zeolite rich clay
St. 1459 G926
brown(10YR4/3) siliceous clay
d.brown(10YR3/3) zeolite rich clay
St. 1460 G927
brown(10YR4/3) siliceous clay
d.brown(10YR3/3) clay
St. 1462 G929
d.brown(10YR3/3) calcareous clay
d.brown(7.5YR3/2) calcareous clay
St. 1463 G930
d.brown(10YR3/3) siliceous clay
d.brown(7.5YR3/2) clay
d.brown(7.5YR3/2) zeolitic clay
cm
Fo Na Di Ra Sp Si Ic Ma Mi
10 30 %
Fo Di Ra Sp Ic Ma Mi

Fig. X-5 (3)

St. 1464 G931

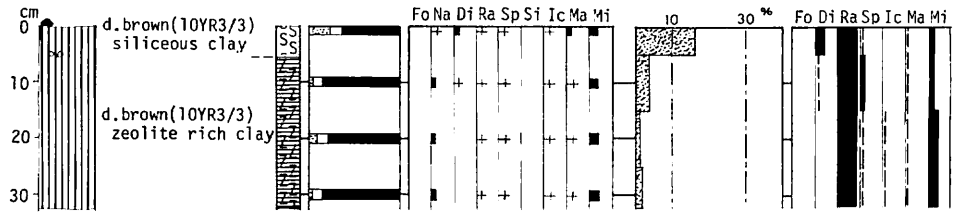

St. 1465 G932

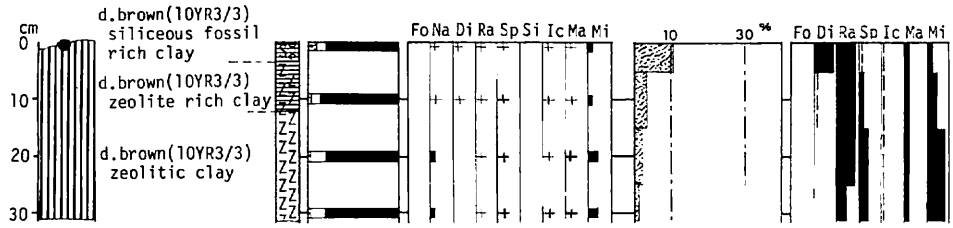

St. 1466 G933

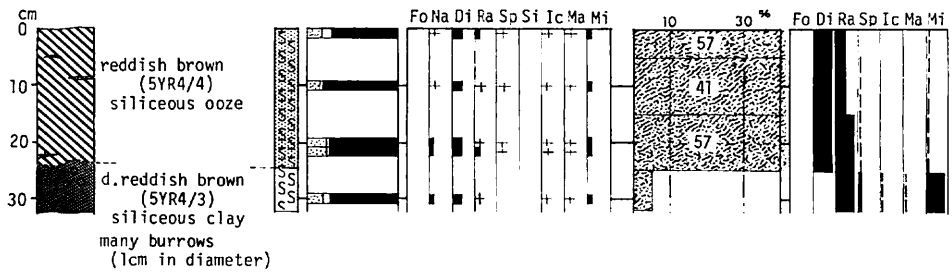

St. 1467 G934

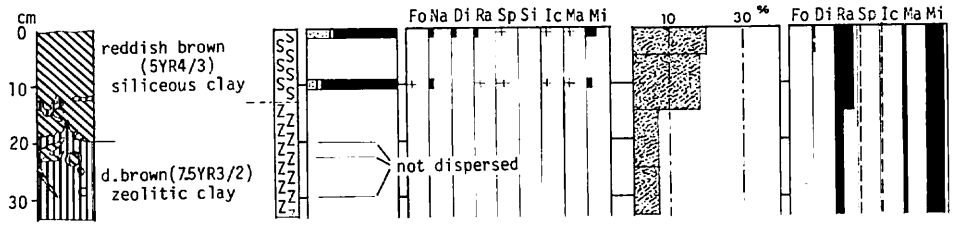

St. 1473 G940

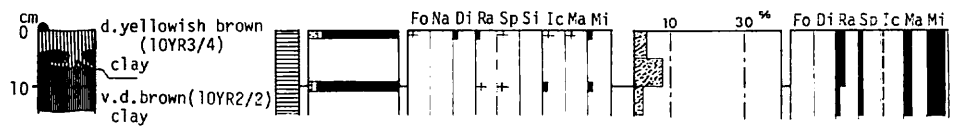

Fig. X-5 (4)

St. 1474 G941

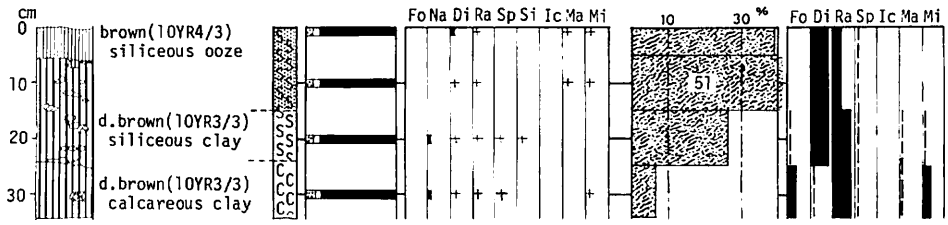

St. 1475 G942

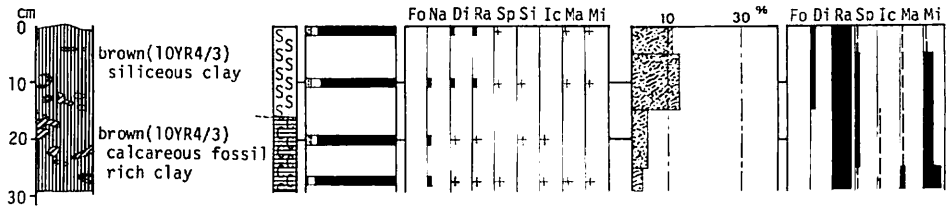

St. 1476 G943

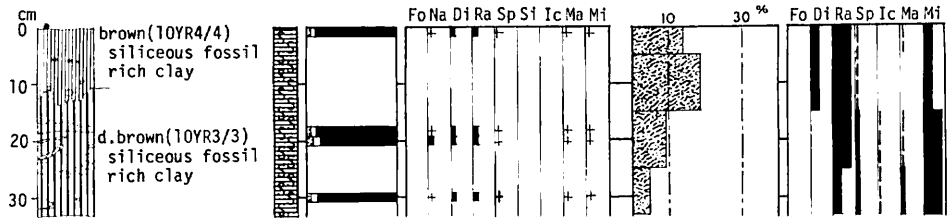

St. 1477 G944

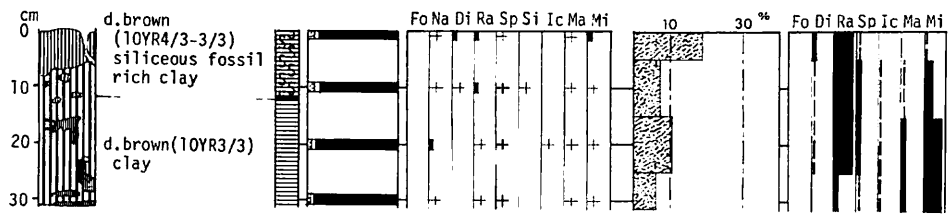

St. 1478 G945

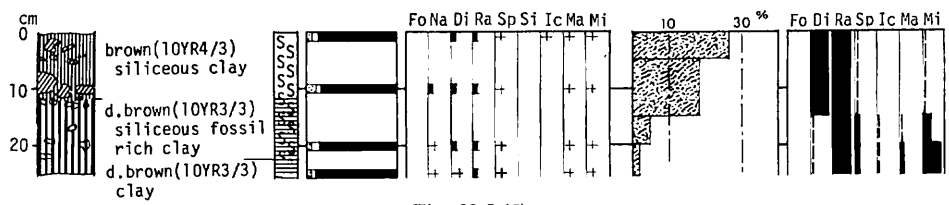

Fig. X-5 (5)

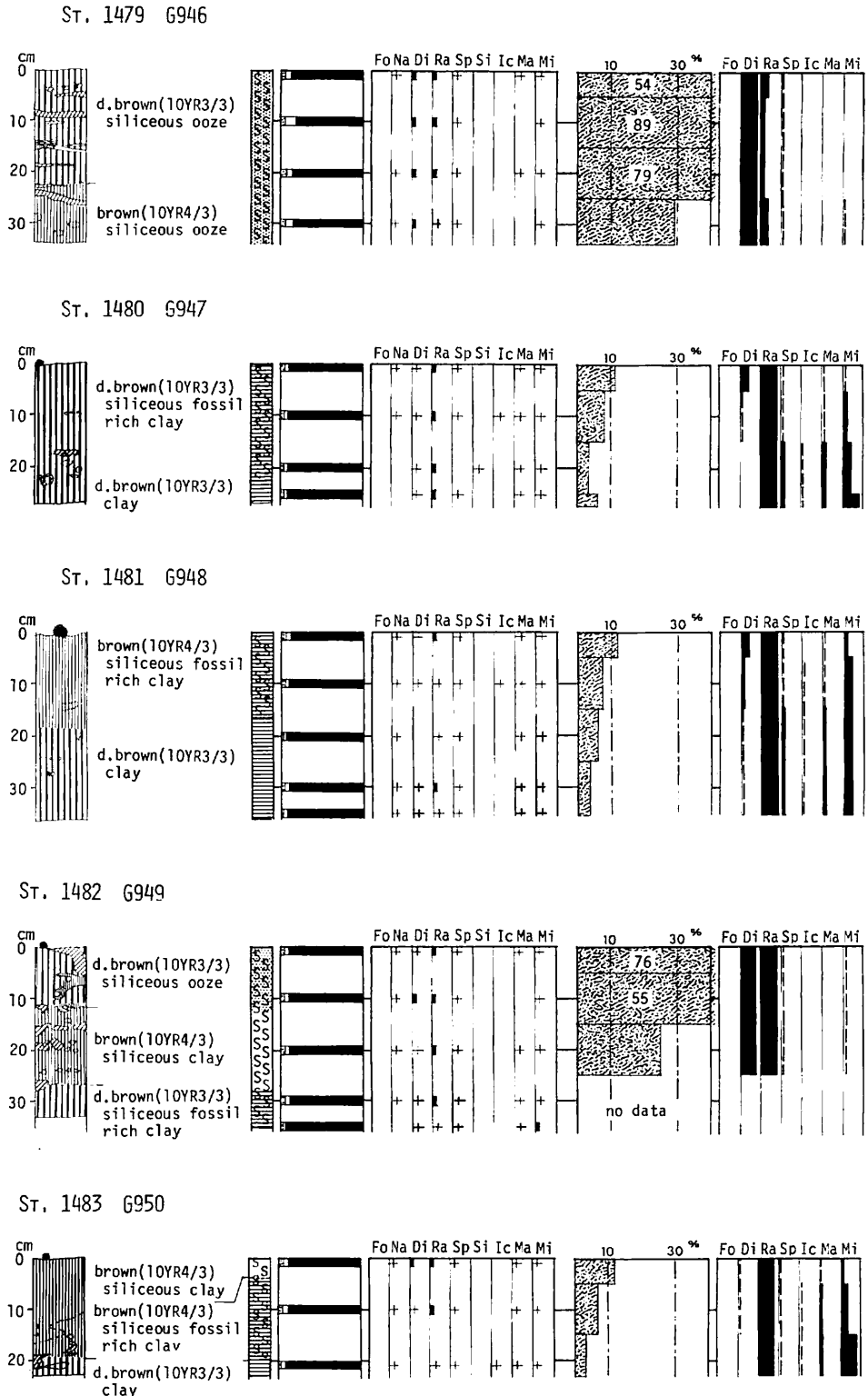
St. 1479 G946
cm
0
10
20
30
d.brown(10YR3/3)
siliceous ooze
brown(10YR4/3)
siliceous ooze
Fo Na Di Ra Sp Si Ic Ma Mi
10 30 %
54
89
79
Fo Di Ra Sp Ic Ma Mi
St. 1480 G947
d.brown(10YR3/3)
siliceous fossil
rich clay
d.brown(10YR3/3)
clay
St. 1481 G948
brown(10YR4/3)
siliceous fossil
rich clay
d.brown(10YR3/3)
clay
St. 1482 G949
d.brown(10YR3/3)
siliceous ooze
brown(10YR4/3)
siliceous clay
d.brown(10YR3/3)
siliceous fossil
rich clay
76
55
no data
St. 1483 G950
brown(10YR4/3)
siliceous clay
brown(10YR4/3)
siliceous fossil
rich clay
d.brown(10YR3/3)
clay

Fig. X-5 (6)

St. 1484 G951

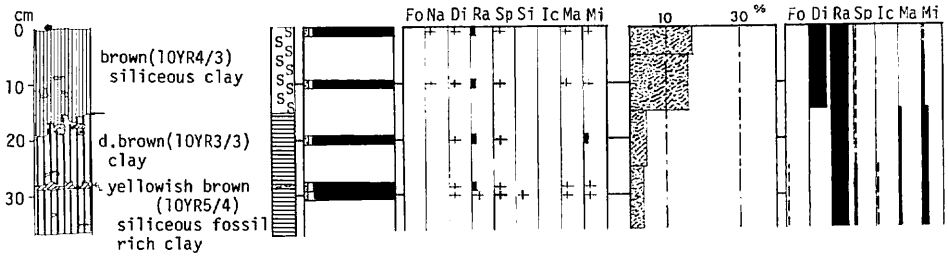

St. 1485 G952

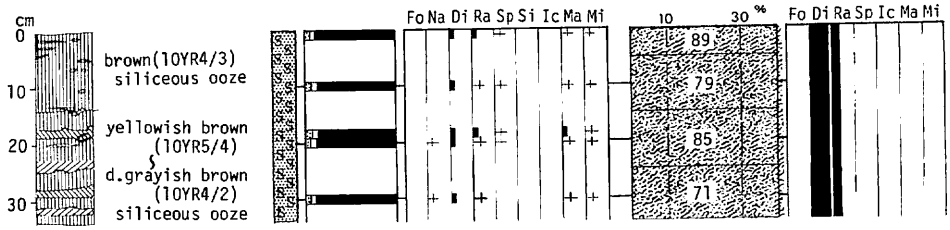

St. 1489 G953

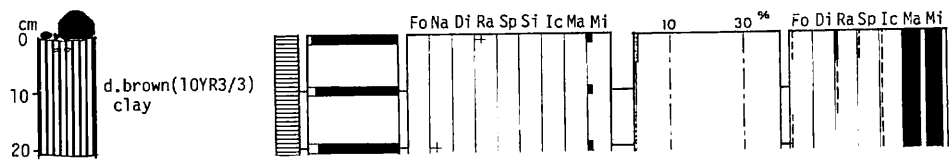

St. 1490 G954

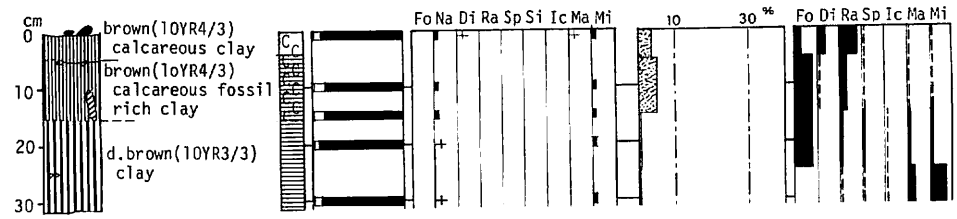

St. 1491 G955

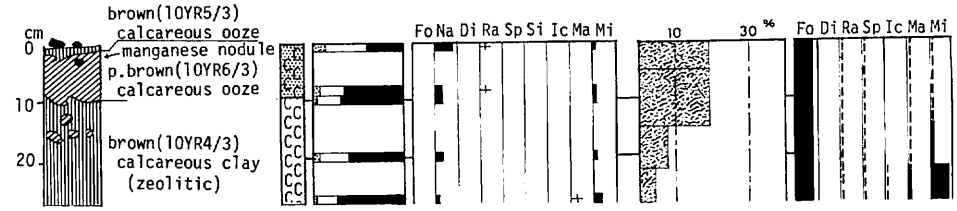

Fig. X-5 (7)

Table X-2 Radiolarians from the surface sediment (0–5 cm) of G930.

Quaternary radiolarians
Collosphaera tuberosa HAECKEL
Siphonosphaera polysiphonia HAECKEL
Lithopera bacca EHRENBERG
Eucyrtidium hexagonatum HAECKEL
Euchitonia spp.
Spongaster tetras EHRENBERG
Dictyocoryne truncatum (EHRENBERG)
Ommatartus tetrathalamus (HAECKEL)
Pterocanium praetextum (EHRENBERG)
Middle Eocene-Oligocene radiolarians*
Periphaena delta SANFILIPPO et RIEDEL
P. decora EHRENBERG
Amphicraspedum prolixum SANFILIPPO et RIEDEL
Eusyringium fistuligerum (EHRENBERG)
Theocampe mongolfieri (EHRENBERG)
Lithochytris vespertilio EHRENBERG
Lychnocanoma babylonis (CLARK et CAMPELL)
Thyrsocyrtis rhizodon (EHRENBERG)
T. bromia EHRENBERG
T. tetracantha (EHRENBERG)
T. triacantha (EHRENBERG)
T. hirsuta (KRASHENINNIKOV)
Podocyrtis goetheana (HAECKEL)
P. chalara RIEDEL et SANFILIPPO
P. papalis EHRENBERG
P. sinuosa EHRENBERG
Dorcadospyris sp.
Lithocyclia aristotelis (EHRENBERG)

*more than 70 per cent of total radiolarians.

The clay of both P140 and P141 contains very little coarse fraction. Some radiolarians occur in this clay but they are reworked.

Pattern of the magnetic polarity change in P141 is well correlated with the magnetic time interval from the Brunhes to the Matuyama Reversed Epoch, and we can assume that the sedimentation rate is constantly 3.1 mm/1,000 y. The base of this core is 1.4 Ma. But the polarity change in P140 is so complicated that a correlation with a time scale is very difficult.

Our results reveal that relatively thin brown clay overlies unconformably on the Paleogene to upper Cretaceous rocks in the area of piston coring.

Basalt fragments were obtained from a seamount of the Line Island Cross Trend ridge (D315) of the southeastern part of this area by chain-bag dredge. And manganese-coated basalt gravel was obtained from the foot of the sea plateau of the western part by freefall grab (FG158C-2). The results of onshore study on these rocks are described in Chapter XXI in this cruise report. Seamounts and sea plateaus which form higher topography may be composed of these kinds of volcanic rocks.

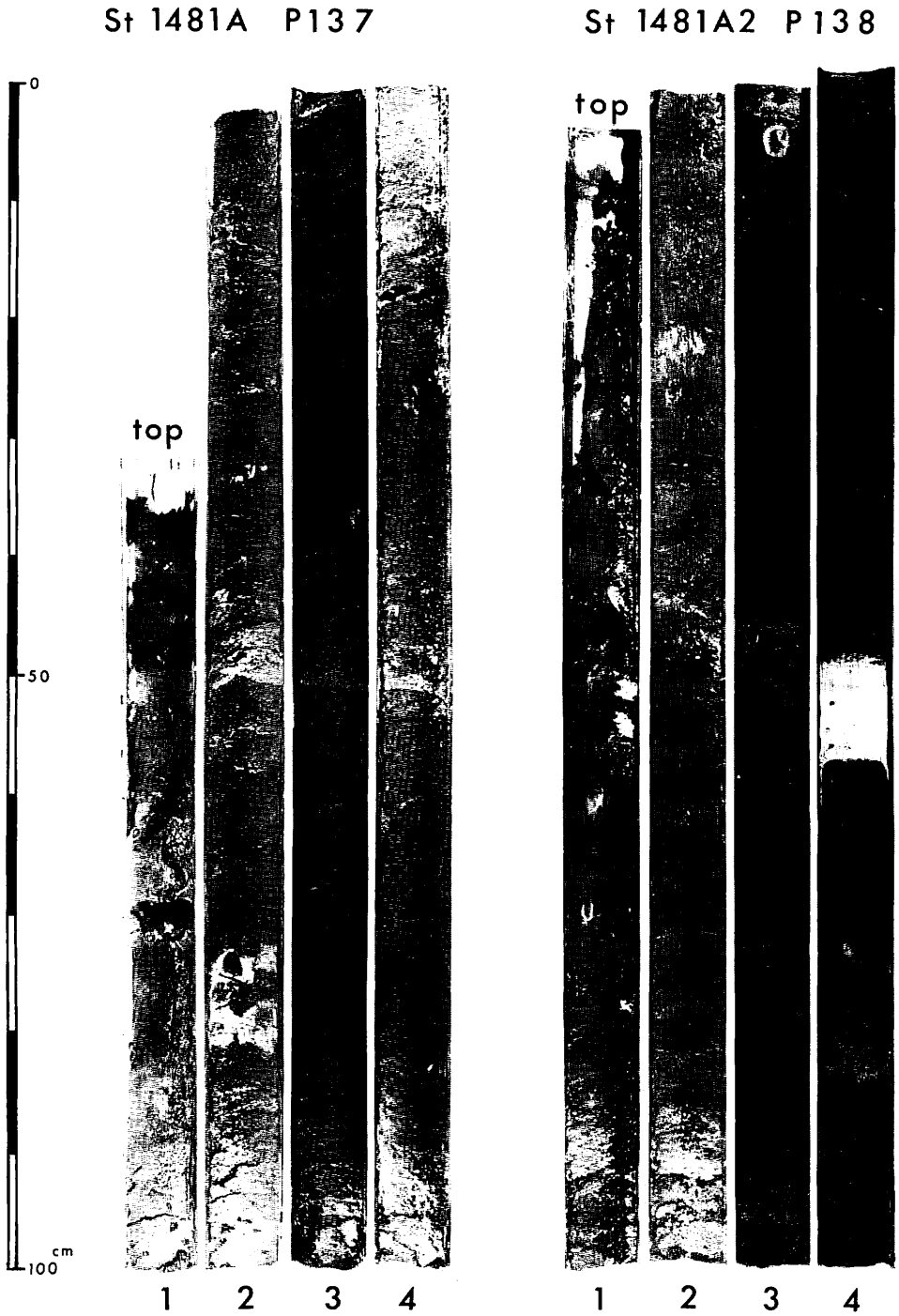

Fig. X-6 (1)

Fig. X-6 Photographs of split surface of piston cores.

Fig. X-6 (2)

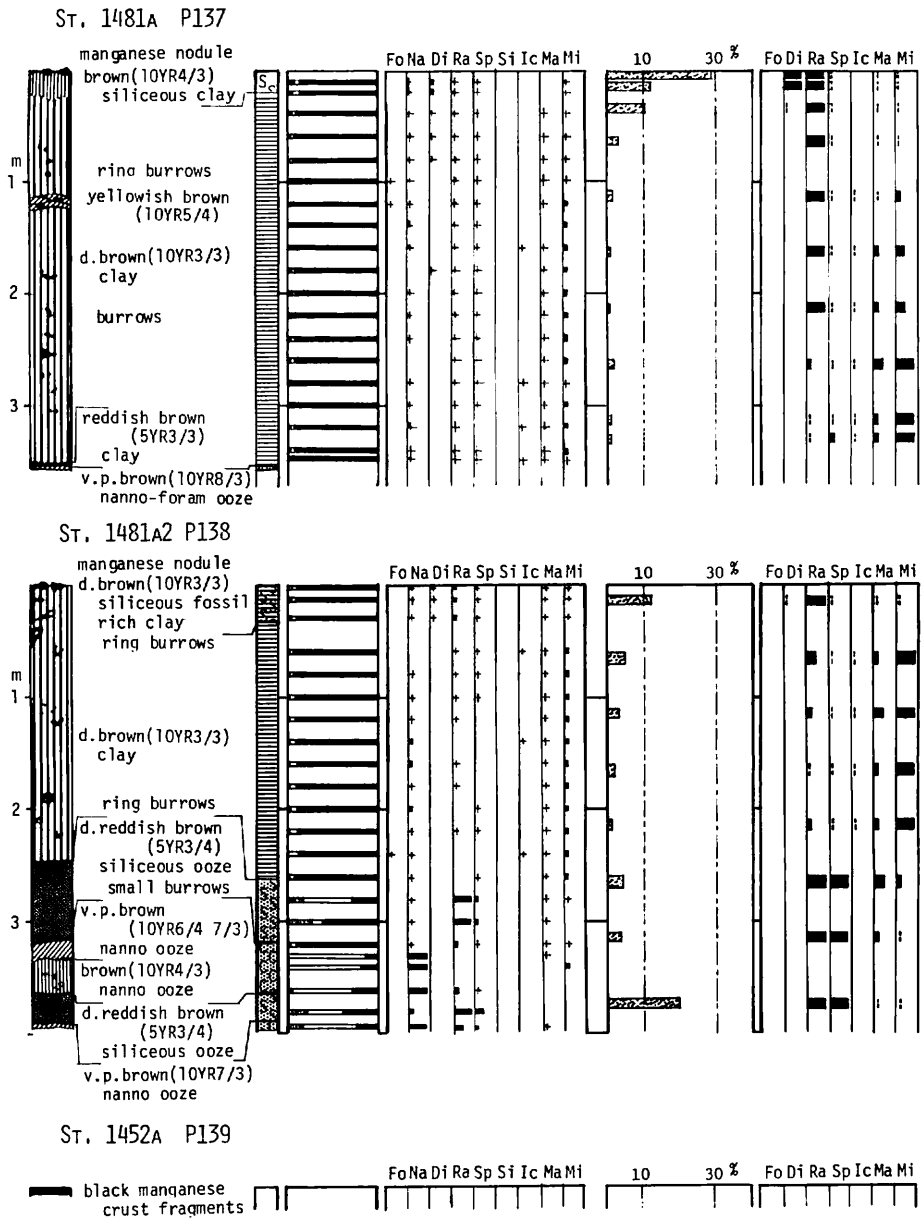

Fig. X-7 (1)

Fig. X-7 Descriptions of piston cores and results of compositional analysis. Legend of this figure is the same as Fig. X-5.

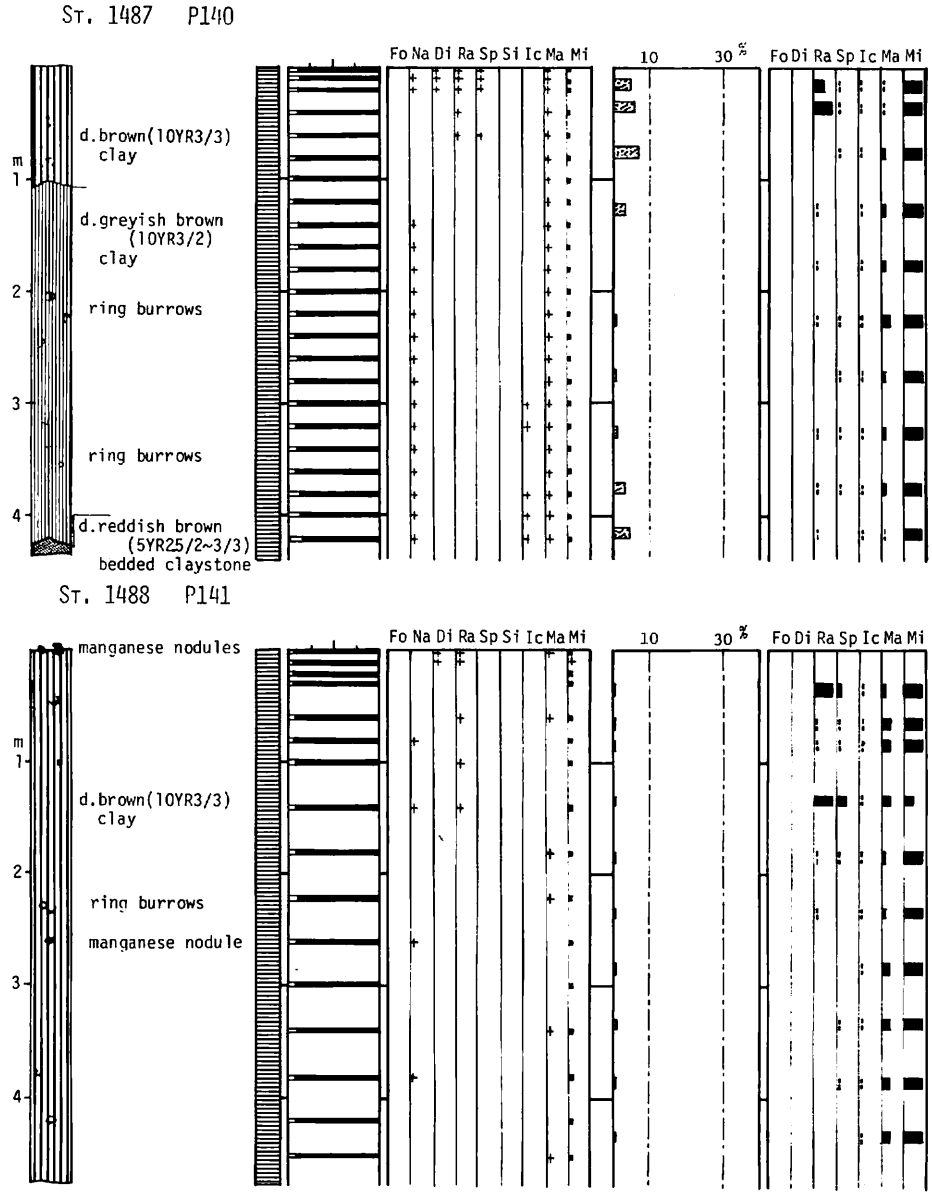
St. 1487 P140
Fo Na Di Ra Sp Si Ic Ma Mi
10
30 %
Fo Di Ra Sp Ic Ma Mi
m
1
2
3
4
d.brown(10YR3/3) clay
d.greyish brown (10YR3/2) clay
ring burrows
ring burrows
d.reddish brown (5YR2.5/2~3/3) bedded claystone
St. 1488 P141
manganese nodules
d.brown(10YR3/3) clay
ring burrows
manganese nodule

Fig. X-7 (2)

Sediments in the detailed survey area

Closely spaced bottom sediment sampling and subbottom profiling were carried out in the detailed survey area for the purpose to reveal the relation among seismic profiles, bottom sediments, and manganese nodule distribution.

The surficial sediment of this area is dominantly the sediments with siliceous organism tests, i.e., siliceous ooze, siliceous clay, and siliceous fossil rich clay (Fig. X-8). A few freefall grab samples show a sparse distribution of calcareous sediments. The sediments rich in siliceous organism tests tend to distribute in the part with thicker surface layer underlain by the continuous opaque horizon on 3.5 kHz record.

In box subcores, coarse fraction materials decrease downward, except for the siliceous ooze samples. This change is due to diminution of siliceous organism tests. The surficial sediments are very likely of the Quaternary from the evidence of Quaternary radiolarians with delicate tests. Some older (mainly Eocene age) radiolarians occur even in the surficial sediment like as the GH79–1 main survey area.

Piston core P138, taken from the western marginal part of this area, is one of the most significant data sources for deducing of geological history of this area. Dark brown

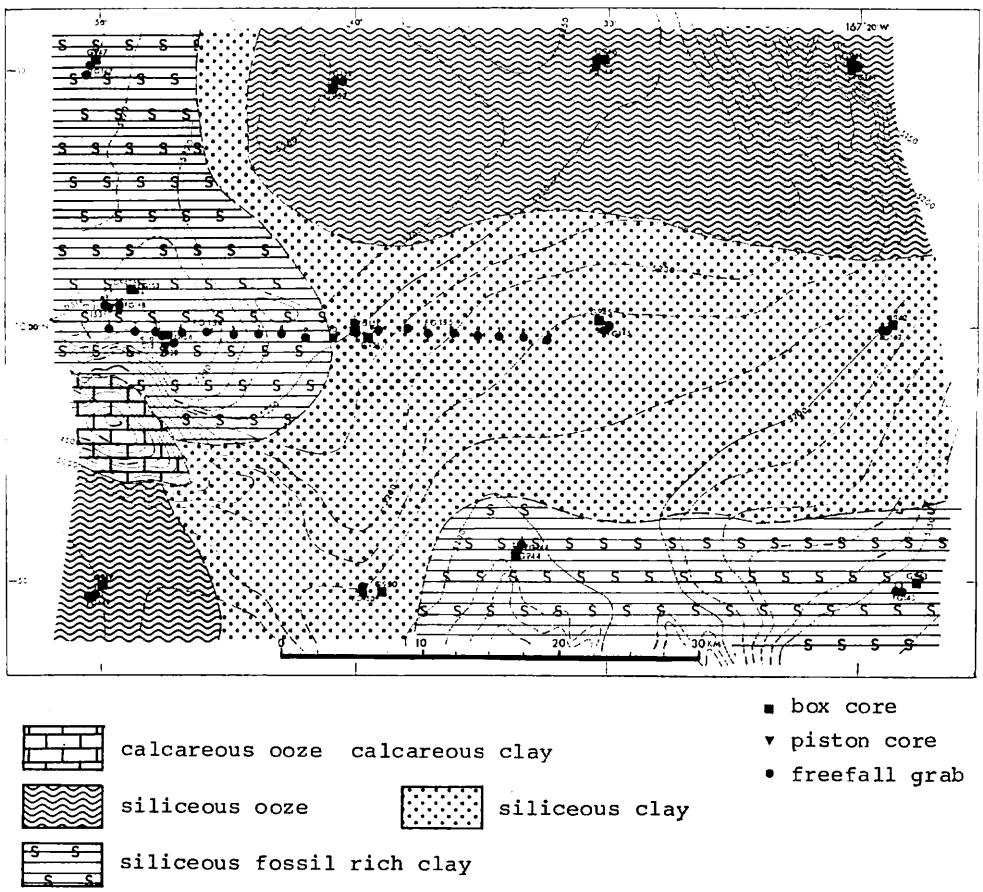

Fig. X-8 Surficial sediment distribution of the detailed survey area.

siliceous fossil rich clay in the part (0–0.3 m) changes to dark brown clay downward. This core shows distinct lithological change at a depth of 2.5 m from the top. The lower part (2.5–3.9 m) is composed of dark reddish brown siliceous ooze with two turbidite layers of very pale brown nannofossil ooze (Fig. X-9). The composition of nannofossil ooze is characterized by the assemblage of the early Miocene (D. BUKRY, personal communication, Table X-3). The siliceous ooze includes a considerable amount of orosphaerid radiolarian spines, which flouished during the Oligocene to the early Miocene. The age assigned by the nannofossil assemblage coincides with that by the radiolarians. Paleomagnetic study of this core shows that the age of the base of the upper clay part is slightly older than the Olduvai Event of the Matuyama Reversed Epoch (ca. 2.0 Ma), assuming that the sedimentation rate of clay is constant with 1.3 mm/1,000 y (JOSHIMA, this cruise report). The lower part of the core appears to be the magnetic Epoch 19 to 20 of the early Miocene, according to the nannofossil data. Between the early Miocene and the late Pliocene, the geological record of about 20 million years is missing in this core.

Core P137 taken near P138 is 3.55 m long and consists of dark brown clay except for the dark brown calcareous rich clay of the top of the core (0–0.2 m) and very pale brown foram-nanno ooze of the core catcher. The composition of the foram-nanno ooze is characterized by the assemblage of the Oligocene nannofossils and planktonic foraminifers (Tables X-3 and X-4). According to the magnetic study (JOSHIMA, this cruise report), the upper part of this core has normal polarity and the lower part has reversed polarity with two short normal polarity portions. Assuming that the sedimentation rate is ca. 3.1 mm/1,000 y, the pattern of magnetic polarity change of upper 2.7 m of this core coincides with the magnetic time scale from the Brunhes to the Jaramillo Event. But the lower short normal polarity portion has no correspondence. The foram-nanno ooze of the core catcher of P137 may belong to the same stratigraphic unit with the turbidite layers of nanno ooze of P138. Though a distinct lithological change as found in P138 is not observed in P137, a hiatus with no large lithological change possibly exist in the lower part of P137.

DSDP Site 165 is situated 300 km southeast of the GH79–1 detailed survey area (Fig. X-2). The late Paleogene to Quaternary sedimentary history at Site 165 (WINTERER, EWING, *et al.*, 1973) seems to be very similar to that in the detailed survey area, as deduced from the data of Core P137 and P138. The geologic history of the present area constructed by both the data is as follows.

In the late Oligocene to the early Miocene, at a larger part of this area clay with abundant siliceous organism tests was deposited under the environment that the depth was deeper than calcium carbonate compensation depth (CCD). The paleolatitude of this area must have been 2° to 3°N at that time (VAN ANDEL *et al.*, 1975). Occasionally turbidites of calcareous ooze were organized into the siliceous sediment sequence. The area was suffered from the strong deep-sea bottom current during the middle Miocene to the late Miocene (or the late Pliocene), and no deposition and/or erosion occurred in this area. This strengthened current is thought to be related to the widespread erosional event associated with the development of a large ice cap on Antarctica around 12 Ma (VAN ANDLE *et al.*, 1975), and the continuous opaque reflection traced in the whole area on the 3.5 kHz profiles is thought to record this sedimentation break.

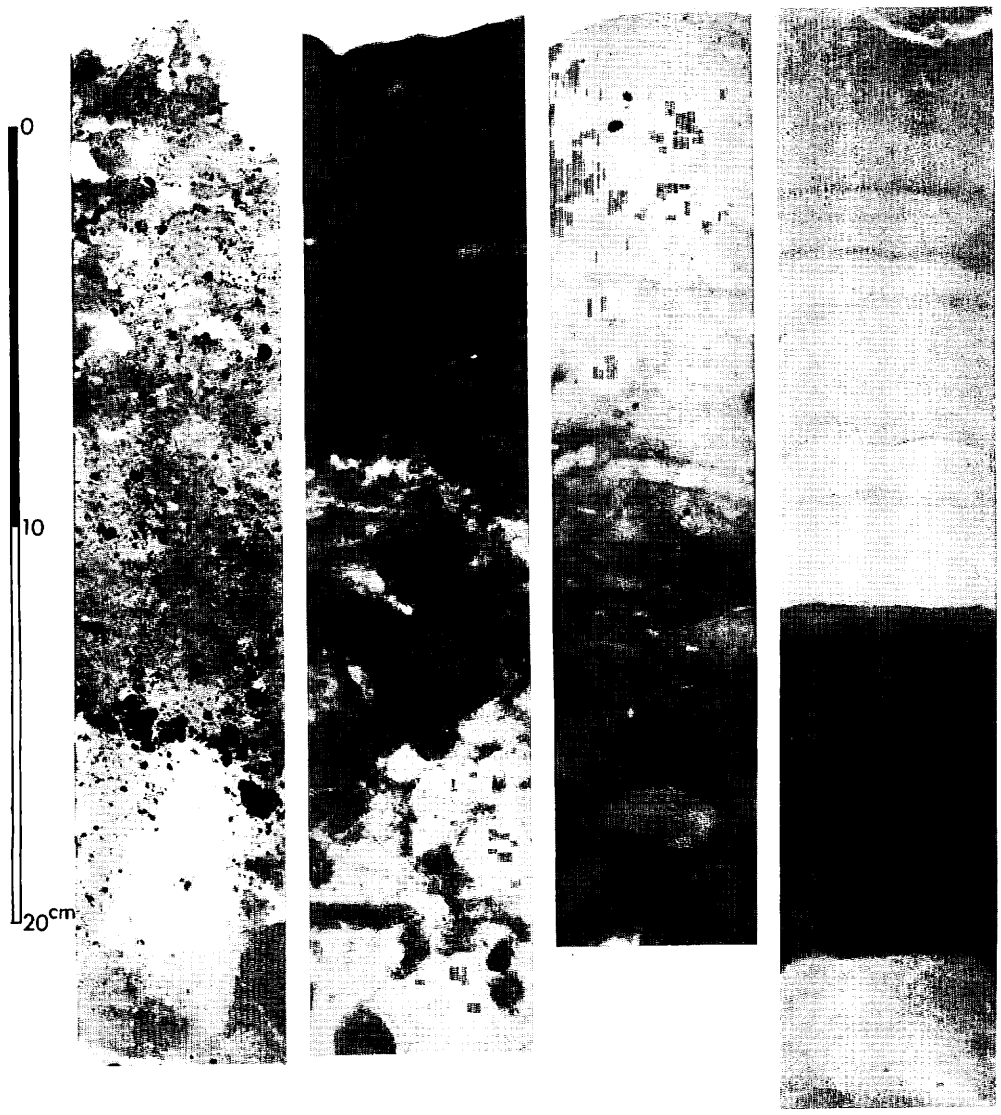

Fig. X-9 X-radiographs of slabs of box core and piston core. **1.** G919. Black spots scattered through the sequence are yellow mineral grains. **2.** G934. Upper darker part is composed of siliceous clay, and lower lighter part of zeolitic clay. **3.** G950. Many burrows are observed in the middle and lower parts. The downward darkening corresponds with the gradual change of the sediment (siliceous clay in the upper part, siliceous fossil rich clay in the middle, and clay in the lower). **4.** P138, 314–342 cm. Darker layer is a turbidite of nanno ooze.

Table X-3 Calcareous nannofossils from P137 and P138 (analyzed by D. BUKRY).

Coccolith species	P-137, 355 cm	P-138, 336–338 cm	P-138, 395 cm
Chiasmolithus altus BUKRY et PERCIVAL	×		
Coccolithus eopelagicus (BRAMLETTE et RIEDEL)	×		
C. miopelagicus BUKRY		×	×
C. pelagicus (WALLICH)	×	×	×
Cyclicargolithus abisectus (MÜLLER)	×		
C. sp. aff. *C. abisectus* (MÜLLER)		×	×
C. floridanus (ROTH et HAY)	×	×	×
Dictyococcites bisectus (HAY *et al.*)	×	*	*
D. scrippsae BUKRY and PERCIVAL		*	
Discoaster deflandrei BRAMLETTE et RIEDEL	×	×	×
Microrhabdulus decoratus DEFLANDRE [Cret.]	*		
Reticulofenestra hillae BUKRY et PERCIVAL	*	*	
R. umbilica (LEVIN)		*	
Sphenolithus ciperoensis BRAMLETTE et WILCOXON	×		
S. conicus BUKRY			×
S. distentus (MARTINI)	×		
S. moriformis BRONNIMANN et STRADNER	×	×	×
S. predistentus BRAMLETTE et WILCOXON		*	
S. pseudoradians BRAMLETTE et WILCOXON		*	
Triquetrorhabdulus carinatus MARTINI		×	×

[×-Present. *-Reworked.] Zones after BUKRY (1975).

P-137, core catcher, 355 cm (10°00.72'N, 167°49.70'W, 5291 m): Late Oligocene *Sphenolithus ciperoensis* Zone, *Cyclicargolithus floridanus* Subzone (early; approx. 25 to 26.5 Ma).

P-138, 336–338 cm (09°59.21'N, 167°47.38'W, 5270 m): Early Miocene *Triquetrorhabdulus carinatus* Zone, *Discoaster deflandrei* Subzone? (approx. 21 to 23 Ma) containing reworked early Oligocene *Helicosphaera reticulata* Zone.

P-138, core catcher, 395 cm: Early Miocene *Triquetrorhabdulus carinatus* Zone, *Discoaster deflandrei* Subzone? (approx. 21 to 23 Ma).

Table X-4 Planktonic foraminifers from P137 (core catcher, 355 cm).

Chiloguembelina cubensis (PALM) group (dominant)
Cassigerinella chipolensis (CUSHMAN et PONTON)
Pseudohastigerina sp.
Globorotalia nana BOLLI
Globorotalia spinulosa CUSHMAN

This assemblage is recognized in the Oligocene sequence at DSDP Site 165.

From the late Pliocene onward, sediments with abundant siliceous organism tests have been deposited in this area and the sediments have changed to clay with less abundant siliceous organism tests at some part of low sedimentation rate.

Benthonic organisms

High activity of benthonic organisms in deep-sea environment of the surveyed area is expressed by lebensspuren and organisms in bottom photographs and split core surfaces.

Table X-5 Lebensspuren and organisms observed in seabed photographs of St. 1481A2 (C-15).

OBSERVED FORM	Figure No. of other reports	Figure No. of this report
Broad groove with closely spaced depressions on each side	24–92 (EWING *et al.*, 1967)	Fig. X-10-1, 9
Narrow grooves, radiating from a small central hole	24–53 (EWING *et al.*, 1967)	Fig. X-10-1, 4
Narrow groove immediately surrounding a lump which bears a central hole	24–28 (EWING *et al.*, 1967)	Fig. X-10-1, 5
Ridge in the pattern of a single spiral	24–3 & 24–4 (EWING *et al.*, 1967) IX-13L (KINOSHITA, 1977)	Figs. X-10-1, 2 & 3
Elongated lump generally resembling a coil (faecal)	24–19 (EWING *et al.*, 1967) VIII-9g (KINOSHITA *et al.*, 1979)	Fig. X-10-1, 1
Ridge distinct from the surrounding bottom (faecal)	IX-13J (KINOSHITA, 1977)	
Holothurian		Fig. X-10-1, 6
Ophiuriod		Fig. X-10-1, 7

Table X-6 Lebensspuren and organisms observed in one-shot photographs.

OBSERVED FORM	Photograph No.	Figure No. of other reports	Figure No. of this report
Lump resembling a crowded rope (faecal)	FG127C-2, 164C-1	IX-11A (KINOSHITA, 1977)	Figs. X-10-2, 2 & 3
Elongated lump generally resembling a coil (faecal)	FG156C-4	VIII-9g (KINOSHITA *et al.*, 1979)	Fig. X-10-2, 1
Ridge resembling a strait or twisted rope (faecal)	FG129C-1, 133C-1, 142C-1, 146C-1, 147C-1, 147C-2, 149C-2, 150C-1, 151C-1, 152C-1, 152C-2, 153C-3, 154C-3, 154C-8, 155C-3, 155C-5, 155C-8, G(B'C)951	IX-13J (KINOSHITA, 1977)	Figs. X-10-2, 4 & 6
Small deep hole (burrow)	FG133C-1, 134C-1, 134C-2, 142C-2, 144C-1		Fig. X-10-2, 5
Fish	FG138C-2		Fig. X-10-2, 7
Starfish	FG154C-8		Fig. X-10-2, 8

Continuous-shot photographs at St. 1481A2 (C-15) show clear images of lebensspuren and organisms (Table X-5). Some of lebensspuren types have already been reported from other G.S.J. cruises in the Central Pacific Basin area (KINOSHITA, 1977; KINOSHITA *et al.*, 1979), and three new types are obtained in the GH79–1 area. One-Shot photographs show only a small amount of lebensspuren, because of their poor images and narrow field of view. All types identified are listed in Table X-6.

In split core surfaces and X-radiographs of core slabs, a large amount of lebensspuren (burrows and mottles) can be found. Sponges and agglutinated foraminifers attached to manganese nodules were observed in box corer (Fig. X-10-3).

Benthonic organisms are considered to have played important roles for vertical mixing of surface sediments, retaining manganese nodules on and/or near sediment surface, and manganese nodule growth.

Summary

1) The GH79–1 main survey area is divided into four provinces by lithology of surficial sediment.
   i) Topographically higher province (shallower than 5,000 m)
      .....calcareous sediment
   ii) Western province (178–173°W)
      .....dark brown clay and zeolitic clay
   iii) Central province (173–169°W)
      .....brown siliceous clay
   iv) Eastern province (169–167°W)
      .....dark brown clay and siliceous fossil rich clay
2) Subcore sequences of box cores show general tendency of downward decrease of siliceous micro-organism tests at 5–20 cm depth.
3) Piston corings along the meridian of 174°W show the development of Paleogene to Cretaceous basement under the surficial sediment layer and low sedimentation rate of surficial sediment.
4) The detailed survey area is dominated by siliceous sediment. It is remarkable that sediment with more siliceous organism tests tends to distribute in the part with thicker surface layer on 3.5 kHz record.
5) Piston corings in the detailed survey area clarify the sedimentary history of this area.
   i) In the late Oligocene to the early Miocene, clay with abundant siliceous organism tests was deposited under CCD. Turbidites of calcareous ooze were organized into siliceous sediment sequence.
   ii) In the middle Miocene to the late Pliocene, the condition of no deposition and/or erosion existed in this area by the strengthened deep-sea bottom current.
   iii) From the late Pliocene onward, sediments with abundant siliceous organism tests have been deposited.
6) The deep-sea photographs and split core surface texture show the high activity of benthonic organisms even in the deep-sea bottom deeper than 5,000 m.

Acknowledgment

Thanks are due to Dr. D. BUKRY, U.S. Geolgical Survey (La Jolla) who kindly studied nannoplankton fossils in piston cores.

References

ARITA, M. (1977) Bottom sediments. *In* MIZUNO, A. and MORITANI, T. (*eds.*), *Geol. Surv. Japan Cruise Report*, no. 8, p. 94–117.

BUKRY, D. (1975) Coccolith and silicoflagellate stratigraphy of northwestern Pacific Ocean, Deep Sea Drilling Project Leg 32. *In* LARSON, R. L., MOBERLY, R., *et al.*,

Initial Repts. of DSDP, vol. 32, p. 667–701.

EWING, M. and DAVIS, R. (1967) Lebensspuren photographed on the ocean floor. *In* HEASEY, J. (*ed.*), *Deep Sea Photograph*, The Johns Hopkins Press, Baltimore, p. 259–294.

KINOSHITA, Y. (1977) Manganese nodules and benthonic activities by deep sea photography. *In* MIZUNO, A. and MORITANI, T. (*eds.*), *Geol. Surv. Japan Cruise Report*, no. 8, p. 78–93.

————, MORITANI, T., and HANDA, K. (1979) Manganese nodule occurrence and benthonic activities observed from deep sea photographs. *In* MORITANI, T. (*ed.*), *Geol. Surv. Japan Cruise Report*, no. 12, p. 106–130.

NAKAO, S. (1979) Bottom sediments. *In* MORITANI, T. (*ed.*), *Geol. Surv. Japan Cruise Report*, no. 12, p. 131–151.

THEYER, F. (1977) Micropaleontological dating of DOMES-project box cores from test areas "A" and "B", tropical Pacific Ocean. *In* PIPER, D. Z. (*ed.*), Deep ocean environmental study: Geology and geochemistry of DOMES sites A, B, and C, Equatorial North Pacific, *U.S.G.S. Open-file Report* 77–778, p. 179–194.

VAN ANDEL, T. H., HEATH, G. R., and MOORE, T. C. Jr. (1975) Cenozoic history and paleoceanography of the Central Equatorial Pacific Ocean. *Mem., Geol. Soc. America*, no. 143, 134p.

WINTERER, E. L., EWING, J. I., *et al.* (1973) *Initial Reports of the Deep Sea Drilling Project*, vol. 17, Washington (U.S. Government Printing Office), xx + 930p.

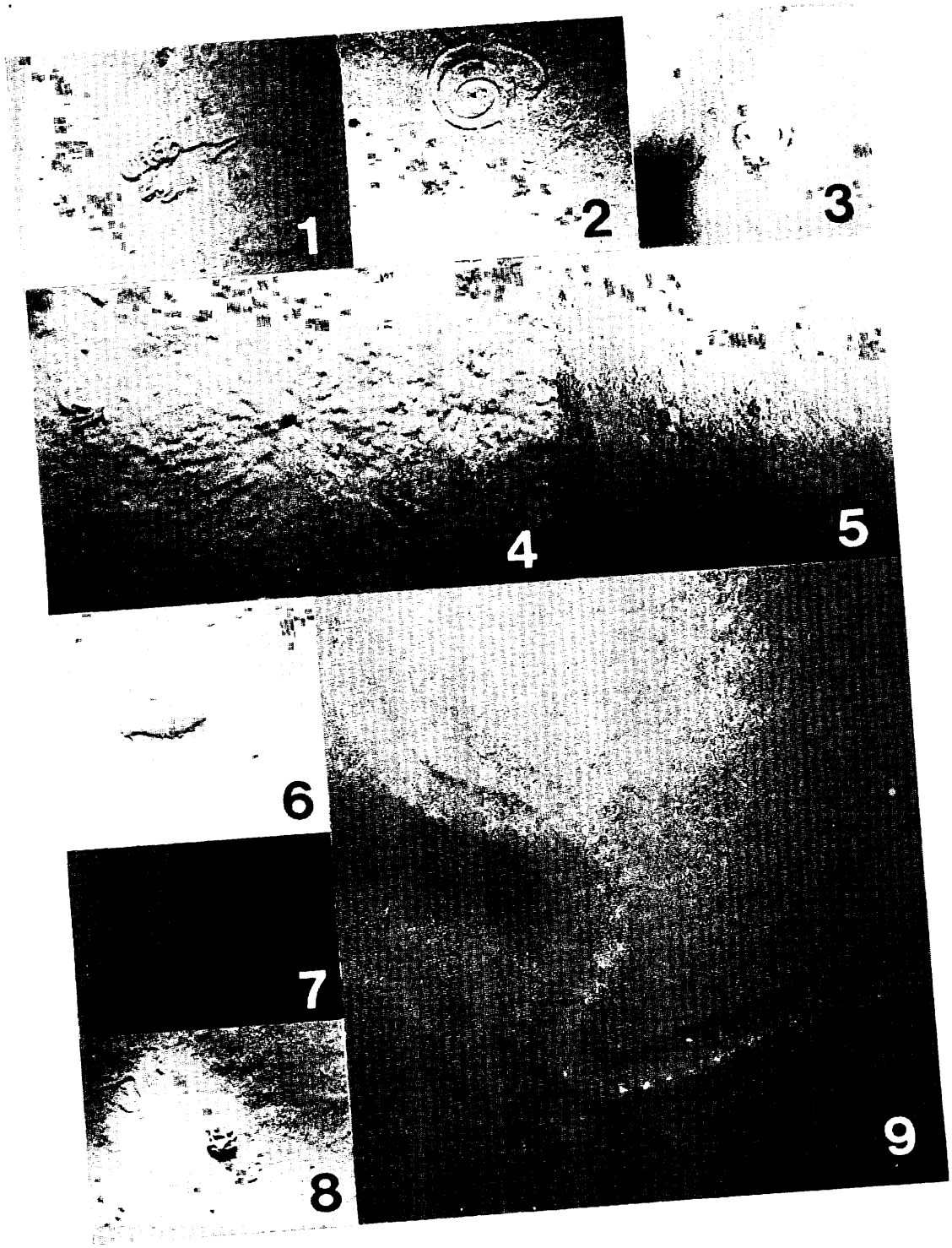

Fig. X-10 Photographs of lebensspuren and organisms.

Fig. X-10-1 Lebensspuren and organisms observed in seabed photographs of St. 1481A2 (C-15).
scale bar = ca. 10 cm
1. Elongated lump generally resembling a coil **2.** Ridge in the pattern of a single spiral **3.** The same type as 2 **4.** Narrow grooves, radiating from a small central hole **5.** Narrow groove immediately surrounding a lump which bears a central hole **6.** Holothurian **7.** Ophiuriod **8.** indeterminable form **9.** Broad groove with closely spaced depressions on each side.

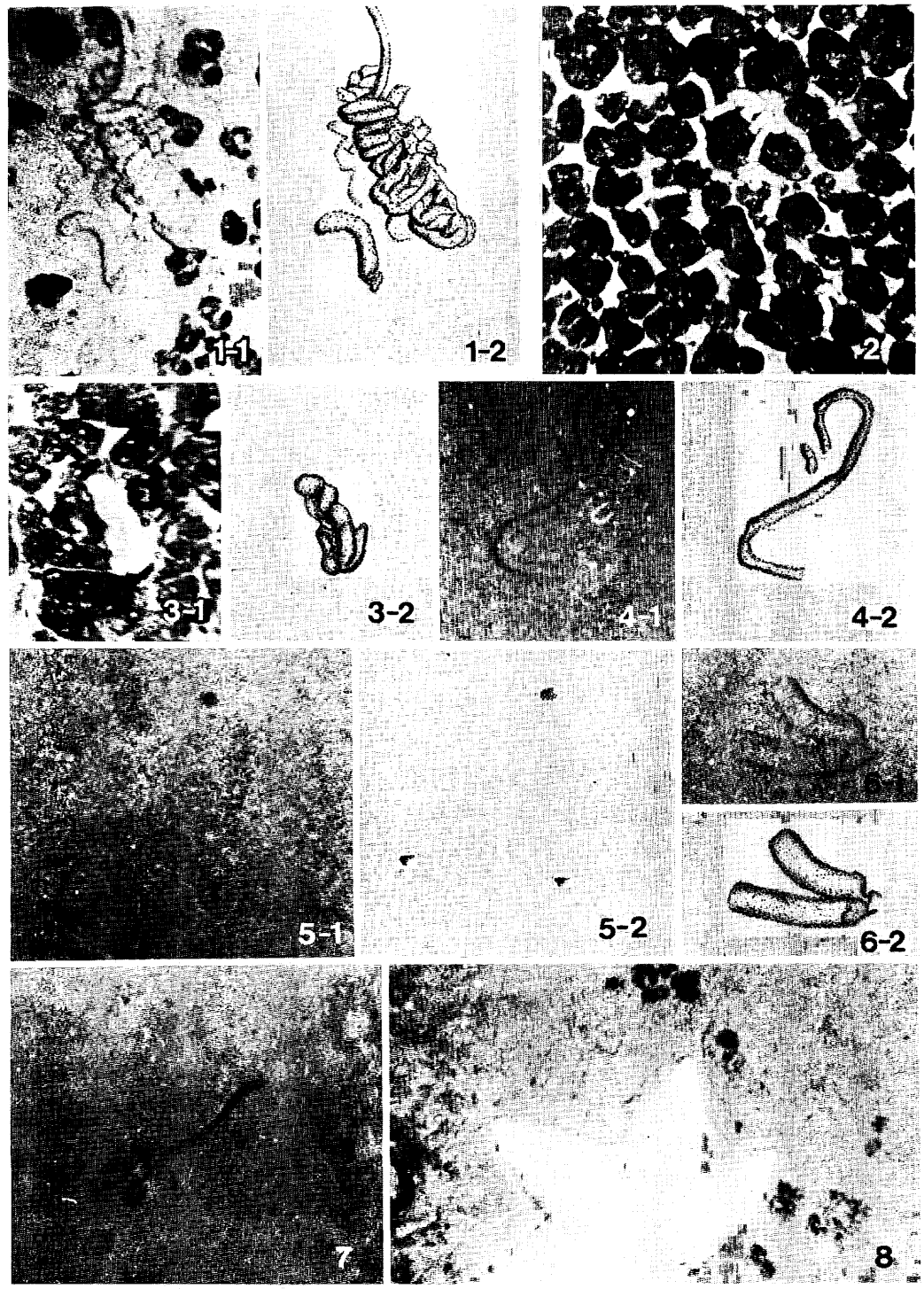

Fig. X-10-2 Lebensspuren and organisms observed in one-shot photographs.
scale bar = ca. 5 cm
1. Elongated lump generally resembling a coil, FG156C-4 **2.** Lump resembling a crowded rope, FG164C-2 **3.** The same type as 2, FG127C-2 **4.** Ridge resembling a twisted rope, FG142C-1 **5.** Small deep holes, FG144C-1 **6.** Ridges, FG155C-8 **7.** Fish, FG138C-2 **8.** Starfish, FG154C-8.

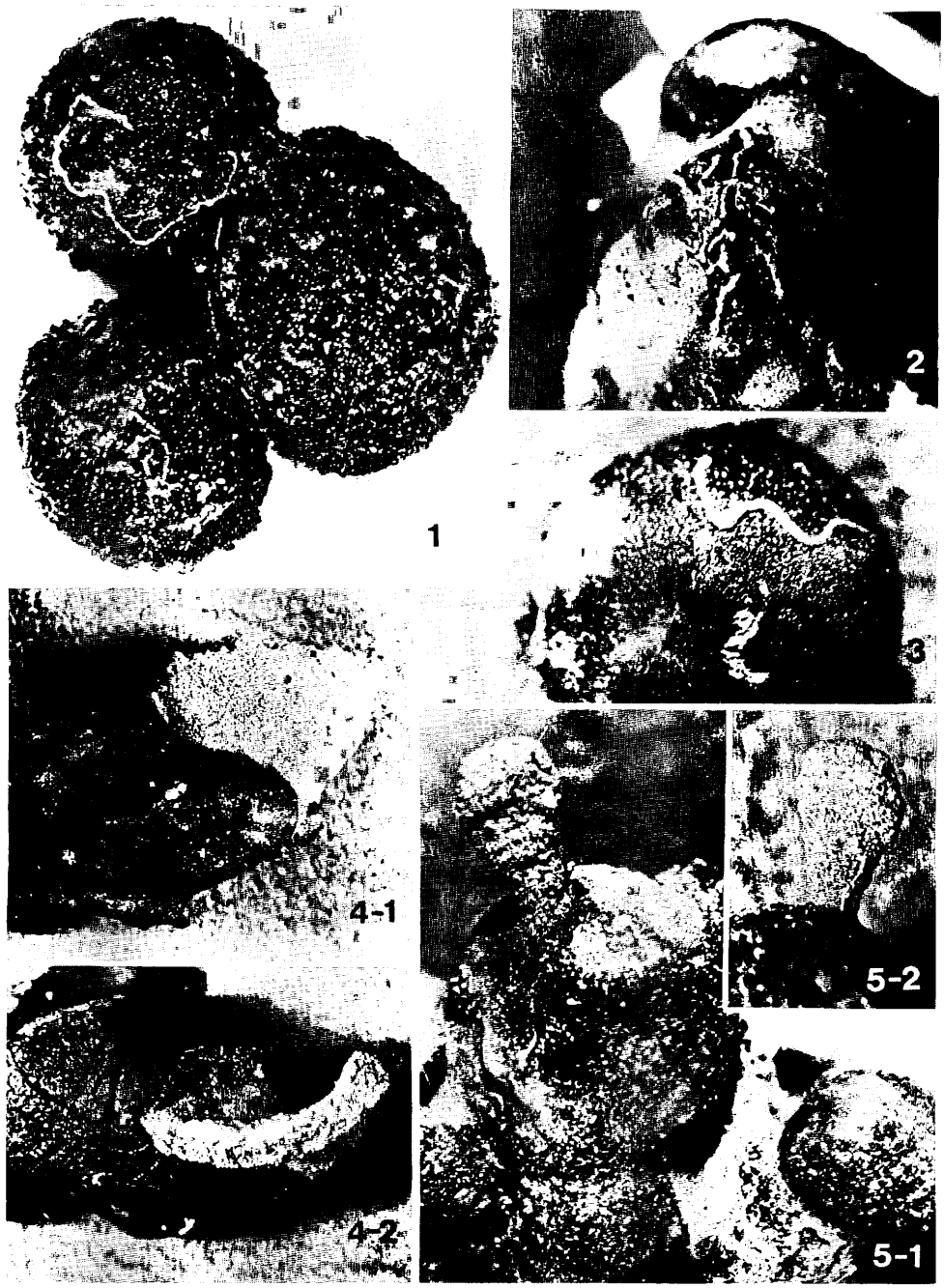

Fig. X-10-3 Organisms on the surfaces of manganese nodules of box core sediment samples.
scale bars = 5 mm
1. Foraminifers, G950 **2.** Foraminifers, G948 **3.** Foraminifer, G948. **4.** Sponge(?), G954. 4–1. side view 4–2. upper view **5.** Sponge(?), G948 5–1. side view 5–2. opposite side view.

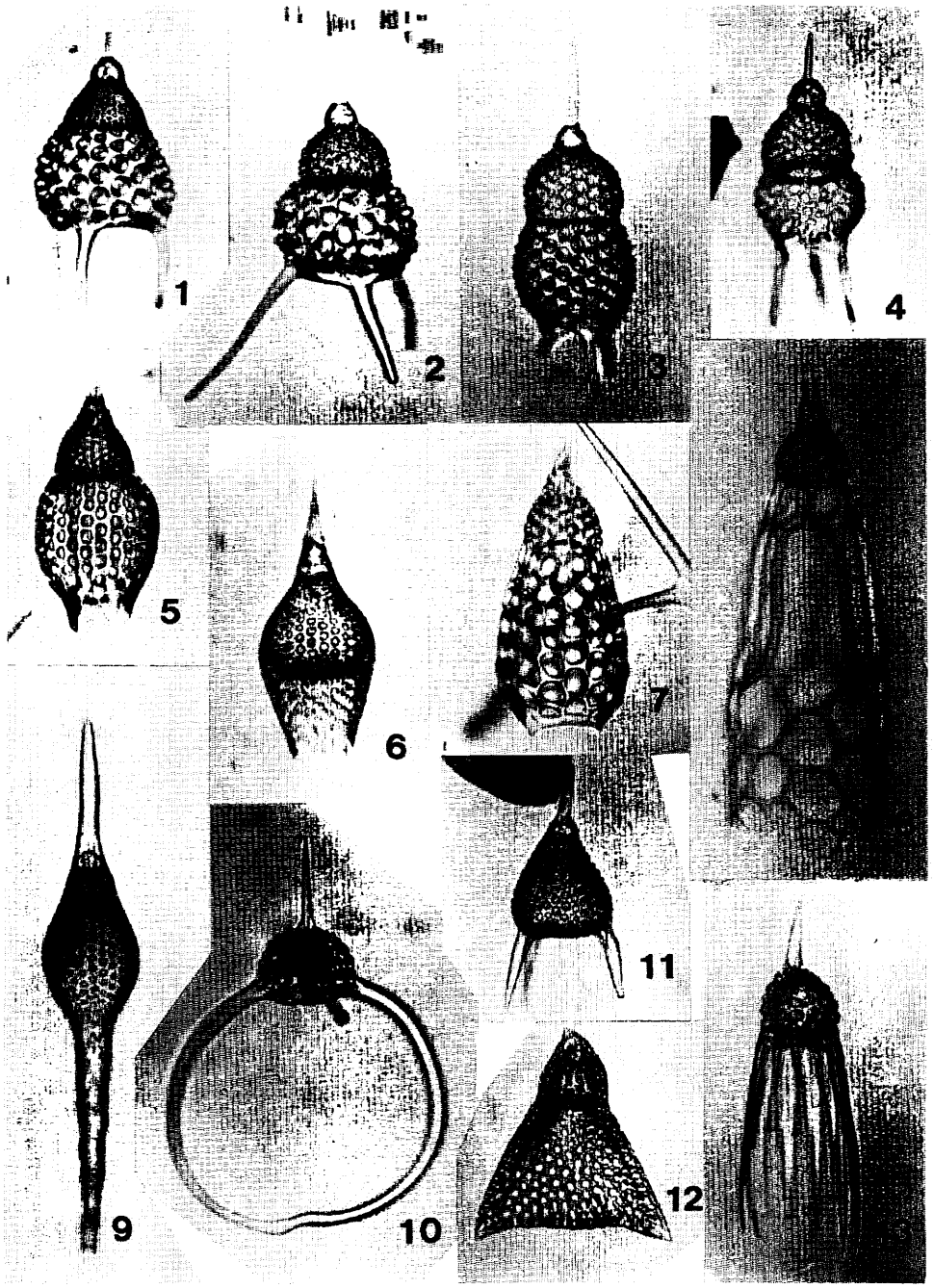

Fig. X-11 Radiolarians, foraminifers, ichthyoliths, and zeolites. scale bars = 100 μ
Fig. X-11-1 Eocene-Oligocene radiolarians occurred in the surface sediment of G930.
1. *Thyrsocyrtis triacantha* (EHRENBERG) **2.** *T. triacantha* (EHRENBERG) **3.** *T. hirsuta* (KRASHENINNIKOV) **4.** *T. hirsuta* (KRASHENINNIKOV) **5.** *Podocyrtis sinuosa* EHRENBERG **6.** *P. papalis* EHRENBERG **7.** *P. chalara* RIEDEL et SANFILIPPO **8.** *P. goetheana* (HAECKEL) **9.** *Eusyringium fistuligerum* (EHRENBERG) **10.** *Dorcadospyris* sp. **11.** *Lychnocanoma babylonis* (CLARK et CAMPELL) **12.** *Lithocyrtis vespertilio* EHRENBERG **13.** Spyrids gen. et sp. indet.

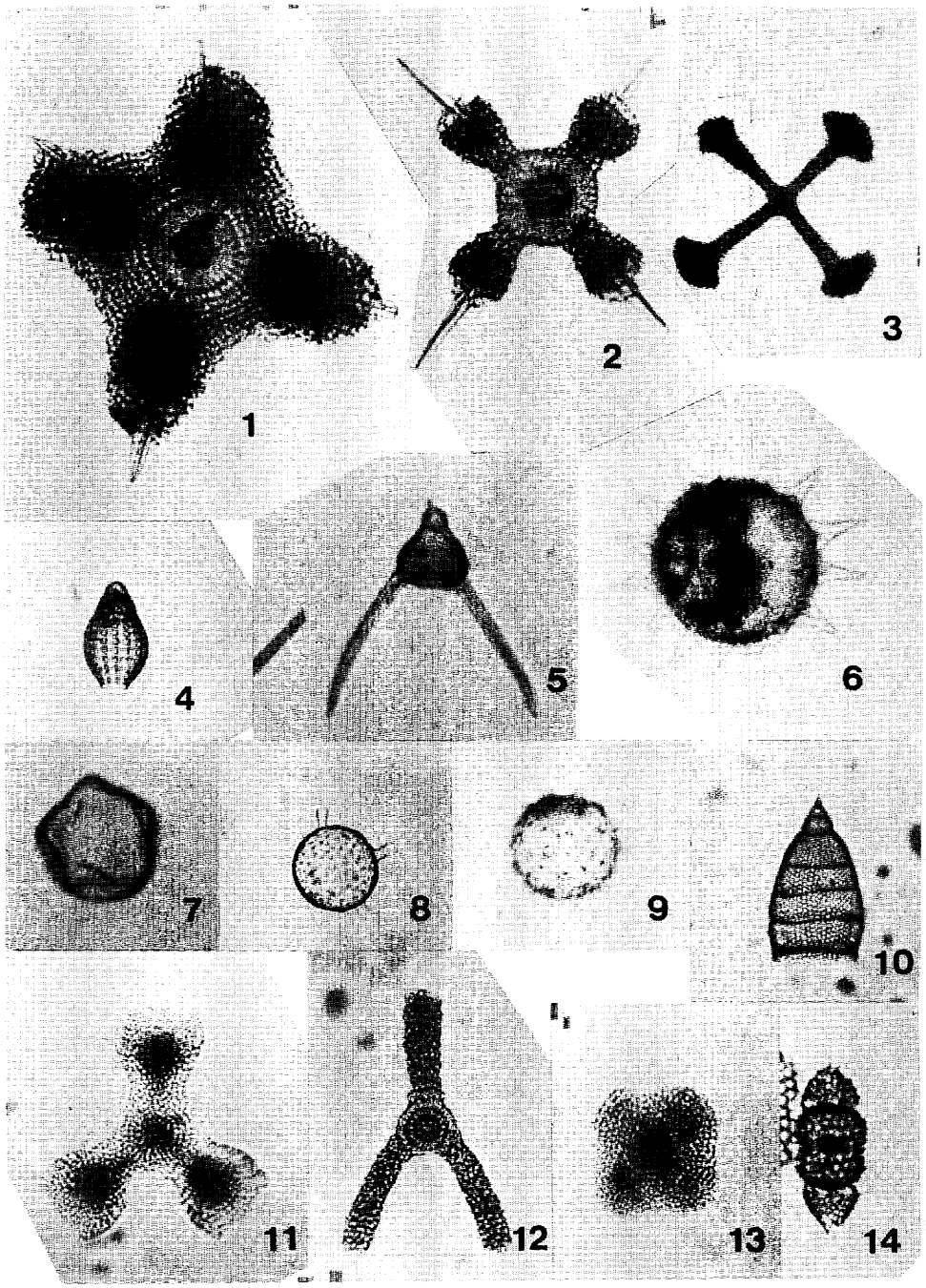

Fig. X-11-2 Eocene-Oligocene radiolarians (1–6) and Quaternary radiolarians (7–14) occurred in the surface sediment of G930.
1. *Lithocyclia* sp. **2.** *L. aristotelis* (EHRENBERG) **3.** *Histiastrum* sp. **4.** *Theocampe mongolfieri* (EHRENBERG) **5.** *Lichnocanoma* sp. **6.** *Periphaena decora* EHRENBERG **7.** *Collosphaera tuberosa* HAECKEL **8.** *Siphonosphaera polysiphonia* HAECKEL **9.** *Polysolenia* sp. **10.** *Eucyrtidium hexagonatum* HAECKEL **11.** *Dictyocoryne truncatum* (EHRENBERG) **12.** *Euchitonia furcata* EHRENBERG **13.** *Spongaster tetras* EHRENBERG **14.** *Ommatartus tetrathalamus* (HAECKEL).

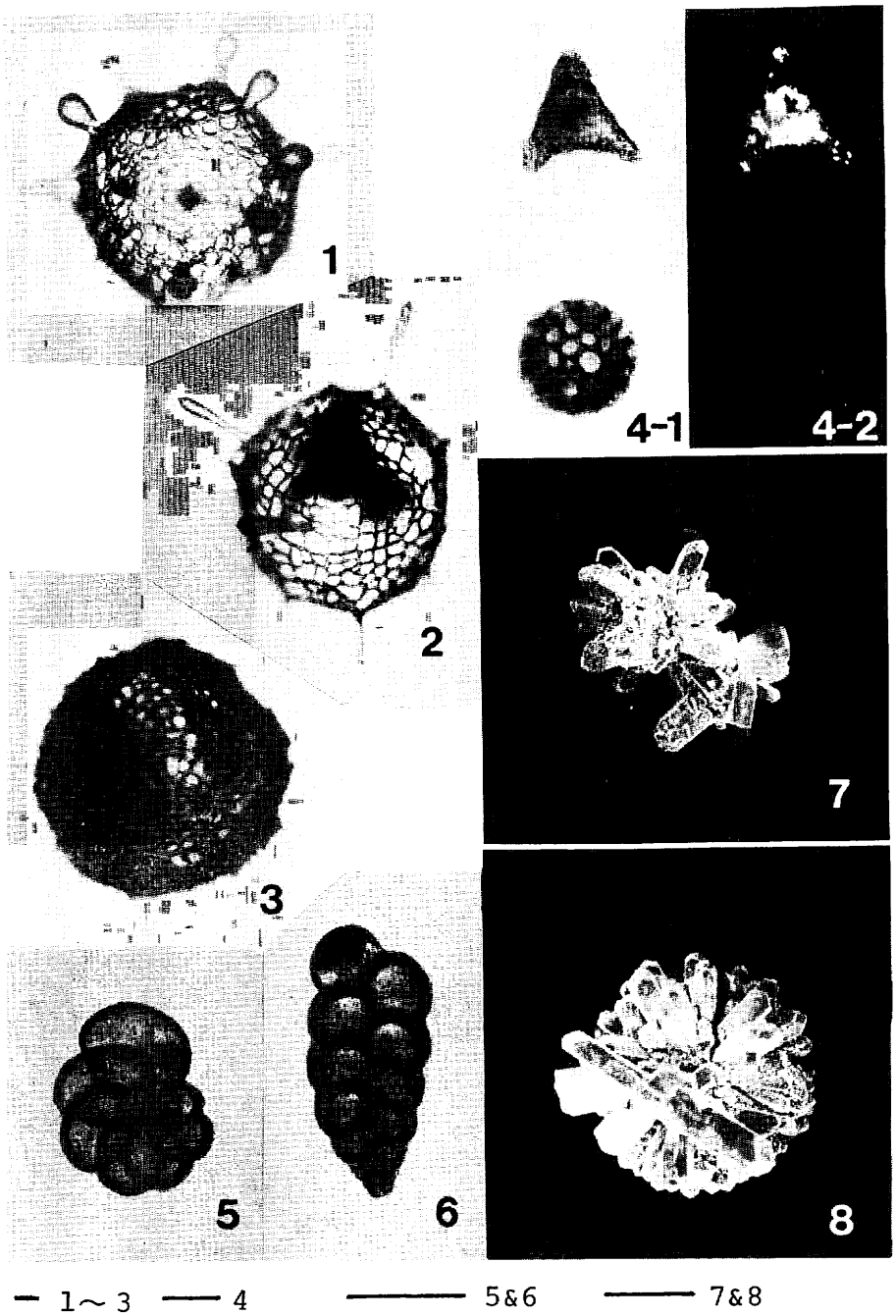

Fig. X-11-3 Radiolarians, foraminifers, and zeolites.
1. *Oroscena gegenbauri* HAECKEL, P138, 260–270 cm **2.** *O.* sp., P138, 260–270 cm **3.** *O. carolae* FRIEND et RIEDEL, P138, 260–270 cm **4.** Crystallized radiolarian (upper, *Lithocyrtis* sp.) and un-crystallized radiolarian (lower, collosphaerid), P140, 410–420 cm. 4–1. parallel nicols 4–2. crossed nicols **5.** *Cassigerinella chipolensis* (CUSHMAN et POLTON), P137, core catcher **6.** *Chiloguembelina cubensis* (PALMER), P137, core catcher **7.** Aggregation of zeolite, P137, 309–318 cm **8.** Aggregation of zeolite, P137, 309–318 cm.

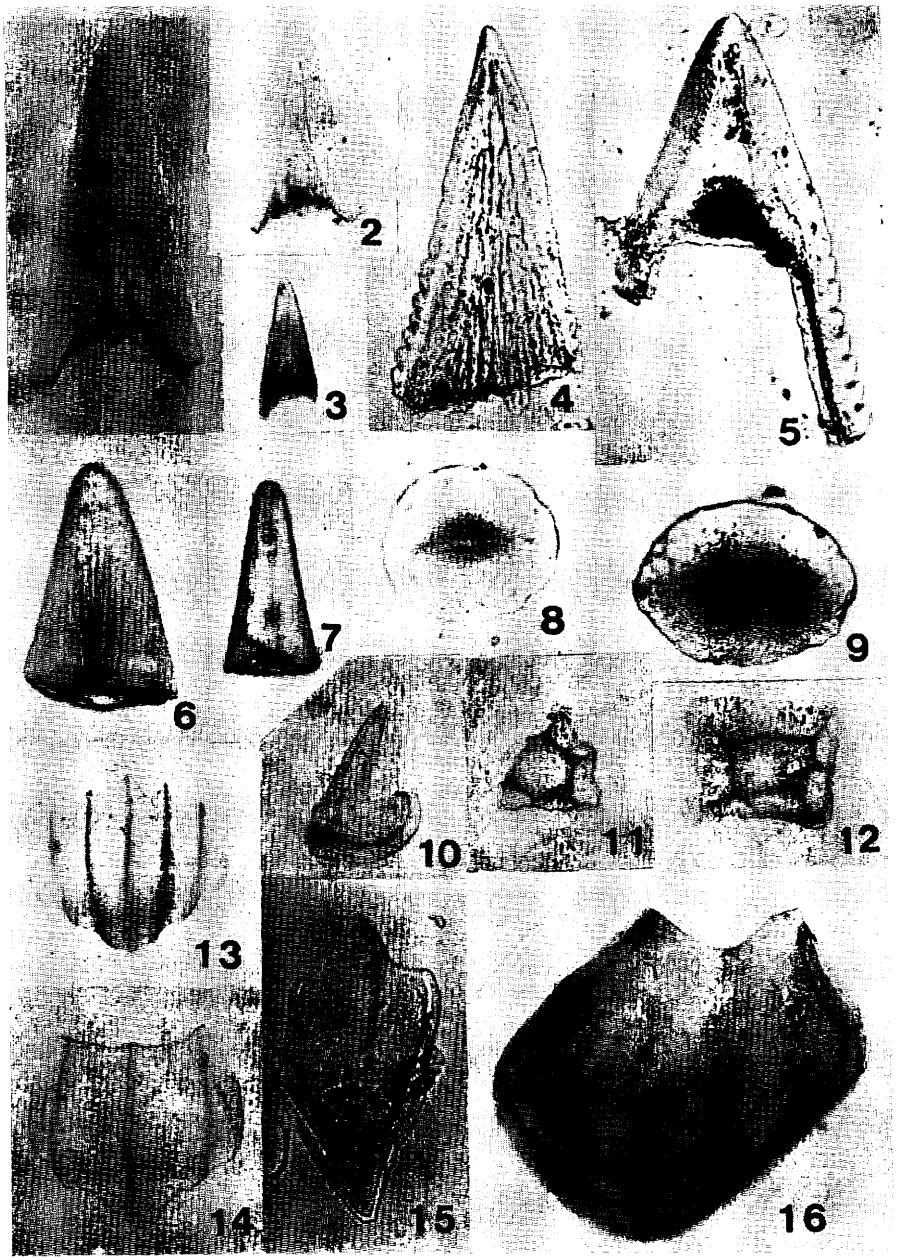

Fig. X-11-4 Ichthyoliths. The explanations of this figure is based on the preliminary observation through the compositional analysis. Further research is needed to get the exact names of ichthyoliths and their biostratigraphic significance.
1. *a9/b1/c1/d1/e1/f1/g1/h1/i2/j2/k2/l0.2/m2/n7/o3/p1*, P140, 410–420 cm. **2.** *a9/b1/c1/d1/e1/f1/g1/h1/i2/j2/k3/l0.2/m1.5/n6/o3/p1*, P138, 309–318 cm. **3.** *a9/b1/c1/d1/e1/f4/g1/h1/i2/j2/k2/l0.5/m2/n7/o1/p1*, P138, 309–318 cm **4.** *a9/b1/c3/d1/e2/f1/g1/h1/i2/j2/k2/l0.1/m2/n1/o1/p1*, P138, 309–318 cm. **5.** *a9/b1/c3/d1/e1/f1/g1/h2/i4/j4/k2/l0.2/m1.1/n5/o1/p1*, P138, 309–318 cm. **6.** *a9/b1/c1/d1/e1/f2/g1/h1/i5/j5/k1/l0.9/m1.5/n1/o1/p3*, P141, 438–440 cm. **7.** *a9/b1/c1/d1/e1/f1/g1/h1/i6/j6/k1/l0.9/m2/n1/o1/p3*, P141, 438–440 cm. **8.** *a5/b4*, P137, 327–334 cm. **9.** *a6/b4*, P141, 438–440 cm. **10.** indeterminable form, P138, 309–318 cm. **11.** *a3/b1*, P138, 309–318 cm. **12.** *a3/b1*, P140, 410–420 cm. **13.** *a2/b2/c5/d2/e1/f1/g1/h3/i1/j1*, P137, 309–318 cm. **14.** *a2/b2/c3/d2/e0/f0/g0/h3/i1/j1*, P137, 309–318 cm. **15.** *a2/b2/c3/d1/e0/f3/g1/h2/i2/j2*, P137, 327–334 cm. **16.** *a3/b1/c4/d3/e0/f2+3/g1+2*, P140, 410–420 cm.